Impact of Quasi-Biennial Oscillation on the northern winter stratospheric polar vortex in CMIP5/6 models

Article in Journal of Climate · February 2020

DOI: 10.1175/JCLI-D-19-0663.1

3 authors:

Jian Rao
Hebrew University of Jerusalem

Chaim I. Garfinkel
Hebrew University of Jerusalem

Ian White
Hebrew University of Jerusalem

Impact of Quasi-Biennial Oscillation on the northern winter stratospheric polar vortex in CMIP5/6 models

Jian Rao[1,2], Chaim I. Garfinkel[1], Ian P. White[1]

[1]Fredy and Nadine Herrmann Institute of Earth Sciences, The Hebrew University of Jerusalem, Edmond J. Safra Campus, Givat Ram Jerusalem 91904, Israel

[2]Key Laboratory of Meteorological Disaster, Ministry of Education (KLME) / Joint International Research Laboratory of Climate and Environment Change (ILCEC) / Collaborative Innovation Center on Forecast and Evaluation of Meteorological Disasters (CIC-FEMD), Nanjing University of Information Science and Technology, Nanjing 210044, China

Revised to *Journal of Climate*

(February 2020)

Corresponding author: Dr. Jian Rao, jian.rao@mail.huji.ac.il

Early Online Release: This preliminary version has been accepted for publication in *Journal of Climate*, may be fully cited, and has been assigned DOI 10.1175/JCLI-D-19-0663.1. The final typeset copyedited article will replace the EOR at the above DOI when it is published.

ABSTRACT

Using 16 CMIP5/6 models with a spontaneously-generated quasi-biennial oscillation (QBO)-like phenomenon, this study investigates the impact of the QBO on the northern winter stratosphere. Eight of the models simulate a QBO with a period similar to that observed (25–31 months), with other models simulating a QBO period of 20–40 months. Regardless of biases in QBO periodicity, the Holton-Tan relationship can be well simulated in CMIP5/6 models with more planetary wave convergence in the polar stratosphere in easterly QBO winters. This wave polar convergence occurs not only due to Holton-Tan mechanism, but also in the midlatitude upper stratosphere where an E-P flux divergence dipole (with poleward E-P flux) is simulated in most models. The wave response in the upper stratosphere appears related to changes in the background circulation through a directly excited meridional-vertical circulation cell above the maximum tropical QBO easterly center. The midlatitude upwelling in this anticlockwise cell is split into two branches, and the north branch descends in the Arctic region and warms the stratospheric polar vortex. Most models underestimate the Arctic stratospheric warming in early winter during easterly QBO. Further analysis suggests that this bias is not due to an overly weak response to a given QBO phase, as the models simulate a realistic response if one focuses on similar QBO phases. Rather, the model bias is due to the too-low frequency of strong QBO winds in the lower stratosphere in early winter simulated by the models.

Key words: Quasi-Biennial Oscillation (QBO); CMIP5/6; stratospheric polar vortex; residual circulation

Accepted for publication in *Journal of Climate*. DOI10.1175/JCLI-D-19-0663.1.

1. Introduction

As a dominant mode of interannual variability in the tropical stratosphere, the Quasi-Biennial Oscillation (QBO) exhibits downward descending zonal winds from the equatorial upper stratosphere to the tropopause every ~28 months with alternating easterlies and westerlies. The QBO is mainly driven by waves of different scales propagating upward that deposit westerly/easterly momentum in the stratosphere (Lindzen and Holton 1968; Andrews and McIntyre 1976; Baldwin et al. 2001). The downward progression of alternating QBO phases occurred without interruption over the observational period before the 2015/16 winter, when the downward propagating westerly phase in the lower stratosphere was disrupted by an unprecedented easterly jet centered at 40hPa, caused by waves transporting momentum from the Northern Hemisphere (NH) (Newman et al., 2016; Osprey et al., 2016; Rao et al. 2017; Watanabe et al. 2018). The easterly phase of the QBO is typically stronger (30–35m s^{-1}) than the westerly phase (15–20m s^{-1}) with maximum amplitude near 20–30hPa (Richter et al. 2014a, 2014b). Many earlier studies revealed that the QBO westerlies are mainly driven by eastward propagating Kelvin waves (Wallace and Kousky 1968; Maruyama 1994; Canziani and Holton 1998). Observational and modelling evidence also show that internal gravity waves excited by convection and frontal systems also contribute to the formation of QBO (Takahashi and Boville 1992; Dunkerton 1997), and are particularly important for the QBO easterlies (Holt et al. 2016).

It has been widely recognized that the QBO can impact the NH winter stratospheric polar vortex, known as the Holton and Tan (1980) relationship (HT relationship hereafter). Holton and Tan (1980) also proposed a mechanism whereby this effect occurs: the QBO modifies the latitude of the zero-wind line at 50 hPa from the near equator to the subtropics between the westerly and easterly QBO (WQBO and EQBO) phases, and therefore changes the width of the extratropical waveguide for upward-propagating planetary waves from the troposphere and their interaction with the stratospheric winds (Baldwin et al. 2001; Anstey and Shepherd 2014).

Accepted for publication in *Journal of Climate*. DOI10.1175/JCLI-D-19-0663.1.

However, this mechanism may not be adequate to explain the entirety of the extratropical response (Garfinkel and Hartmann 2011a, 2011b; Garfinkel et al. 2012; Watson and Gray 2014; White et al. 2015, 2016; Rao et al. 2019a).

The influence of the QBO on the NH winter surface climate was reviewed by Baldwin et al. (2001) and Anstey and Shepherd (2014). The NH stratospheric polar vortex may impact the European surface, the Siberian High and East Asian winter monsoon through the projected Northern Annular Mode or Arctic Oscillation (NAM/AO) (Thompson and Wallace 2000; Gong et al. 2001), which can bridge the tropical QBO and the extratropical climate variations. Therefore, the stratospheric polar vortex can mediate the QBO and surface conditions (Baldwin and Tung 1994; Ruzmaikin et al. 2005; Marshall and Scaife 2009). Other routes communicating the QBO with the extratropics also include the impact of the QBO-induced direct meridional circulation on the subtropical jet (Randel et al. 1999; Garfinkel and Hartmann 2011a, 2011b; Garfinkel et al. 2012; White et al. 2015), and the direct influence of the QBO on tropical deep convection and the related teleconnections spanning tropics and extratropics (Collimore et al. 2003; Liess and Geller 2012; Yoo and Son 2016; Son et al. 2017; Gray et al. 2018).

Via the above routes, the QBO can also modulate the redistribution of the stratospheric aerosol, water vapor, ozone, and other chemical substances (Randel and Wu 1996; O'Sullivan and Dunkerton 1997; Luo et al. 1997; Randel et al. 1998; Choi et al. 1998; Dunkerton 2001; Kawatani et al. 2014), the Indian summer monsoon (Claud and Terray 2007), and even typhoon/hurricane tracks over the western Pacific (Ho et al. 2009). Similar to impacts of the QBO on the NH, the linkage between the QBO and the Southern Hemisphere (SH) has also been analyzed (Baldwin and Dunkerton 1998; Naito et al. 2002). For example, the QBO can affect the deceleration of the SH polar night jet from August to November and therefore the SH final warming (Naito et al. 2002).

Accepted for publication in *Journal of Climate*. DOI10.1175/JCLI-D-19-0663.1.

Models which lack a QBO cannot simulate any of these aforementioned processes, and only in the last twenty years have general circulation models been successful in representing the QBO. Early representation of the QBO was achieved in two-dimensional models (Politowicz and Hitchman 1997; Jones et al. 1998), in simplified general circulation models (GCM) (Horinouchi and Yoden 1998), and in the comprehensive GCM CCSR/NIES by Takahashi (1996, 1999), with two different horizontal resolutions (T21L60 and T42L60 with a model top at 0.5hPa; vertical resolution: 500m). Finer horizontal resolutions in the ECMWF model (T63 and T159) were also tested by Untch et al. (1998). Similarly, Giorgetta et al. (2002, 2006) found that a vertical resolution of 700m (L90 with model top at 0.01hPa) and a horizontal resolution of T42 (~2.8°) together with parameterized gravity wave drag are adequate to simulate the QBO in the MAECHAM5 model. Furthermore, Scaife et al. (2000) showed that the QBO is present in the Met Office Unified Model with an adequate amount of momentum flux from parameterized gravity waves. Only five models (CMCC-CMS, MPI-ESM-MR, HadGEM2-CCS, MIROC-ESM-CHEM, MIROC-ESM) from the Coupled Model Intercomparison Project Phases 5 (CMIP5) can reproduce the QBO-like phenomenon in the tropics, and a long-term decreasing trend of the QBO amplitude from 70–10hPa and an enhanced Brewer-Dobson circulation under the global warming background are found in those models (Kawatani and Hamilton 2013; Butchart et al. 2018).

More recently there has been a rapid increase in the number of models that are capable of simulating a spontaneous QBO, and sufficiently fine vertical resolution (<1000 m) in the lower stratosphere has been identified as a crucial ingredient (Boville and Randel 1992; Richter et al. 2014a; Solomon et al. 2014; Anstey et al. 2016; Butchart et al. 2018). For example, a vertical resolution of 500m and adequate gravity wave drags are needed to obtain a realistic QBO in the modified CAM5 model increased to 60 levels (L60CAM) (Richter et al. 2014a, 2014b) as compared to CAM5 with 700m or 1200m vertical resolution. The QBO can be adequately

Accepted for publication in *Journal of Climate*. DOI10.1175/JCLI-D-19-0663.1.

represented with horizontal resolution of ~200 km as long as vertical resolution of the model is fine enough (Richter et al. 2014a, 2014b). The QBO is more dependent on vertical rather than horizontal resolution (Giorgetta et al. 2006; Richter et al. 2014a). Rind et al. (2014) reported that the QBO has been generated in the two GISS coupled models through parameterizing gravity waves associated with model convection and improving the vertical resolution. Similar results are also seen in Geller et al. (2016): an adequate amount of momentum flux from gravity waves and a fine vertical resolution are necessary to simulate a realistic QBO in GISS-E2 models.

Several metrics of the QBO in CCMVal2 (Chemistry-Climate Model Validation Activity, phase 2) models and CMIP5 models have been assessed, including the squared amplitude and the period (Schenzinger et al. 2017; Butchart et al. 2018). However, the Atmospheric Model Intercomparison Project (AMIP)-type simulations in previous studies usually show a much less robust and less consistent EQBO minus WQBO composite in the extratropics in CCMVal2 and CMIP5 models (Butchart et al. 2018; Naoe and Yoshida 2019). Causes for a poor HT relationship in CMIP5/CCMVal2 experiments might include (1) shortness of data available (Naoe and Yoshida 2019); (2) nonlinear interactions with the 11-year solar cycle (Salby and Callaghan 2000; Camp and Tung 2007; Labitzke and Kunze 2009; Matthes et al. 2010; Scaife et al. 2013; Andrews et al. 2015; Gray et al. 2016; Rao and Ren 2017, 2018; Rao et al. 2019a), El Niño-Oscillation (ENSO) SST anomalies (Garfinkel and Hartmann 2007; Wei et al. 2007; Bell et al. 2009; Calvo et al. 2009; Ineson and Scaife 2009; Weinberger et al. 2019; Rao and Ren 2016; Rao et al. 2019b) and atmospheric internal variation in the AMIP-type run; (3) lack of interactive chemistry module and ozone feedbacks (Silverman et al. 2018; Naoe and Yoshida 2019); and (4) insufficient improvements of the non-orographic gravity wave parametrization (Rind et al. 2014; Geller et al. 2016; Naoe and Yoshida 2019). In contrast, some of the models

Accepted for publication in *Journal of Climate*. DOI10.1175/JCLI-D-19-0663.1.

participating in the seasonal to subseasonal (S2S) project appear to simulate a HT effect statistically indistinguishable from that observed (Garfinkel et al. 2018c).

Some pilot studies based on individual CMIP6 models have been recently published. For example, Naoe and Yoshida (2019) reported that the modelled influence of the QBO on nearby regions in one of the CMIP6 models, i.e., MRI-ESM2-0, is highly consistent with the reanalysis, including the E-P flux divergence/convergence dipole between the midlatitude mid-to-upper stratosphere and the subpolar lower-to-mid stratosphere. The westerlies above the equatorial QBO easterly center (30–50hPa) arch downward and poleward to the 30–40°N lower stratosphere, where an enhanced upward propagation of waves is observed and modelled. Using another model, HadGEM3-GC2, Andrews et al. (2019) show that the observed AO response to QBO is clearly identified in the model.

Compared with the AMIP-type experiments that usually have a relatively short time length, the historical run in CMIP5/6 datasets is usually much longer (156 years for CMIP5 and 165 years for CMIP6). However, the HT relationship between the QBO and the stratospheric polar vortex in atmosphere-ocean coupled simulations has not been systematically assessed for CMIP5 and especially CMIP6 models. In this study, we aim to systematically evaluate the QBO and its influence on the NH extratropics, based on a century and half of historical simulation produced with 16 coupled climate models participating in CMIP5/6. The interference of other factors with the QBO's impact in short observational record and short AMIP-type simulations can be minimized when we have a long enough data record. A large sample size can robustly assess the HT relationship in models.

This study mainly focuses on the following three questions: (1) Of the increasingly large number of CMIP5/6 models that can reproduce a QBO-like phenomenon, how many simulate the HT relationship? (2) Is the planetary wave response to the QBO similar in CMIP5/6 models and observations, and what is the seasonality (early winter vs late winter) of the HT relationship

Accepted for publication in *Journal of Climate*. DOI10.1175/JCLI-D-19-0663.1.

in CMIP5/6 models as compared to observations? (3) Are the atmospheric response patterns during different phases of the QBO successfully simulated in models? If so, how many models? The structure of the paper is organized as below. Following the introduction in this section, section 2 describes the CMIP5/6 models and methods employed in this study. The evaluation of the QBO representation in models is shown in section 3. Section 4 introduces the HT relationship in models and its seasonality, followed by a finer assessment of the HT relationship in eight different QBO phases in section 5. The seasonal evolution of the modelled HT relationship is discussed in section 6. Finally, section 7 presents a summary and conclusion.

2. Model datasets and methods

2.1 CMIP5/6 models with QBO-like signals

Table 1 shows 16 models used in this study, including 7 CMIP5 models (from CESM1-WACCM to MPI-ESM-MR) and 9 CMIP6 models (from BCC-CSM2-MR to UKESM1-0-LL). Four of the 7 CMIP5 models were used by Kawatani and Hamilton (2013), specifically, HadGEM2-CCS, MIROC-ESM-CHEM, MIROC-ESM, and MPI-ESM-MR. The first model, CESM1-WACCM, cannot spontaneously generate the QBO and is nudged toward the observation by relaxing equatorial zonal winds between 86 and 4hPa to observed QBO varying in time with an approximate 28-month period (Matthes et al. 2010; Marsh et al. 2013). Two other CMIP5 models, CMCC-CMS and GEOSCCM released their data relatively late, and hence were not used in Kawatani and Hamilton (2013). The historical run for the GEOSCCM model is unavailable, but a 230-yr coupled run with the greenhouse gas and ozone-depleting substance forcings fixed at 1950 levels is available (Li et al. 2016; Garfinkel et al. 2018a, 2018b). All the CMIP5 models have a model top above 0.01hPa and have at least 60 vertical levels. Historical experiments from those “high-top” (i.e., the model top pressure< 1hPa; this threshold was also used in Charlton-Perez et al. (2013)) CMIP5 models have also been widely

Accepted for publication in *Journal of Climate*. DOI10.1175/JCLI-D-19-0663.1.

used to explore the stratospheric ENSO teleconnections (Hurwitz et al. 2014; Calvo et al. 2017; Rao et al. 2019b) and sudden warming frequency(Charlton-Perez et al. 2013).

At the time of writing 20 models had submitted data for the CMIP6 historical experiment (May 2019). The evolution of the equatorial (5°S–5°N) zonal winds in all those CMIP6 models were analyzed, and at least 9 CMIP6 models can reproduce a QBO-like phenomenon in the tropical stratosphere. Out of those 9 CMIP6 models that have a QBO, 8 of them are high-top models, and only one is a low-top (i.e., the model top pressure ≥ 1hPa) model (BCC-CSM2-MR). Note that the L60CAM model, which has been shown to successfully reproduce the QBO (e.g., Richter et al. 2014a; Solomon et al. 2014), is also a low-top model. All QBO-resolving CMIP6 models have at least 23 vertical levels from 100–1 hPa. The horizontal resolution in CMIP6 models is generally higher than in CMIP5 models, though a finer horizontal resolution appears less important than a finer vertical resolution to simulate the QBO (see the introduction). The first historical experiment is available for nearly all CMIP5/6 models in Table 1 except the GEOSCCM, which has a 230-yr control experiment with the external forcing fixed at 1950. The affiliation, nationality, horizontal resolution, model top and levels, and reference for each model are listed in Table 1.

2.2 Methods

There are at least two methods to define the QBO in previous studies, one based on a single pressure level, and the other based on two different time series. On one hand, the HT relationship was originally identified using a single-level QBO index, QBO30 or QBO50 (Holton and Tan 1980; Gray et al. 1992; Baldwin et al. 2001; Garfinkel and Hartmann 2007). The QBO30 index is the zonal mean zonal wind anomalies (i.e., deseasonalized and detrended data) at 30 hPa about the equator (5°S–5°N), and the QBO50 is similar but using winds at 50hPa. A second commonly used methodology of studying the extratropical response to QBO is to use a pair of QBO indices to better characterize the QBO phase and vertical structure. At

Accepted for publication in *Journal of Climate*. DOI10.1175/JCLI-D-19-0663.1.

least four different pairs of indices have been used: (1) the 15-hPa and 30-hPa QBO index (Andrews et al. 2019); (2) the vertical shear index of two-level zonal winds (Huesmann and Hitchman 2001; White et al. 2015, 2016); (3) an empirical orthogonal function (EOF) analysis of the full QBO structure, which leads to two dominant EOFs that succinctly describe QBO variability (Wallace et al. 1993; Randel et al. 1999; Anstey et al. 2010; Solomon et al. 2014; Schenzinger et al. 2017; Gray et al. 2018; Rao and Ren 2017, 2018); and (4) ensemble empirical mode decompositions (EEMD) of QBO30 and its tendency (Huang et al. 2012; Hu et al. 2012). The definition of the QBO phase based on the EOF1 of the equatorial zonal-mean zonal winds is very similar to QBO30 or QBO50 for the NH composites and the 25-hPa wind for the SH composites (Baldwin et al. 2001).

In observations, there is considerable variability in the QBO period, amplitude, and vertical structure, due to both intrinsic nonlinearity and interference from other processes (Huang et al. 2012; Hu et al. 2012). For example, the westerlies move downward faster than the easterlies, and the easterly phase lasts longer than westerly phase at higher levels while the reverse is true at lower levels. The QBO easterly winds are generally stronger than westerly winds. Due to asymmetries in temporal evolution (e.g., WQBO winds last longer than EQBO winds in the lower stratosphere) and spatial structure of the QBO, the selected WQBO size is usually much larger than the EQBO size based on the 50-hPa zonal wind. In addition, some models largely underestimate the QBO magnitude in the lower stratosphere, and for some models the QBO is difficult to detect at 50 hPa. To avoid such artificial asymmetry in selected WQBO and EQBO sizes and a small sample size for models using lower stratospheric winds, the winter-mean (December–February) QBO30 index is used in this study because the westerly phase lasts nearly as long as the easterly phase at 30 hPa. The WQBO and EQBO winter sizes for the ERA-Interim (Dee et al. 2011) and JRA55 (Kobayashi et al. 2015) reanalyses and CMIP5/6 models are listed in Table 2, where we can still find the size asymmetry in many models

Accepted for publication in *Journal of Climate*. DOI10.1175/JCLI-D-19-0663.1.

(EQBO/WQBO ratio<1). We use a uniform criterion for reanalyses and models to define QBO phases: the WQBO winter is selected if the winter-mean QBO30 exceeds 5 m s^{-1}, and the EQBO winter is selected if the winter-mean QBO30 falls below –5 m s^{-1}. We also assessed sensitivity by using the standard deviation of QBO30 as the threshold for each model, but the composite pattern was nearly unchanged (not shown). The composite for EQBO and WQBO is very similar but with the sign reversed, and only EQBO minus WQBO difference (a larger equivalent sample size than either of the two QBO phases) is shown in the paper. The two-sided Student's t-test is adopted to assess the statistical significance of the difference between the WQBO and EQBO composites, and the autocorrelation (R_{xx} or R_{yy}) for the variable of interest (x or y) is also incorporated in the calculation of the effective degrees of freedom (EDOF), $\mathrm{EDOF} = \frac{n}{\sum_{j=-\infty}^{\infty} R_{xx}(j) R_{yy}(j)}$, where n is the sample size, $R_{xx}(j) = \frac{1}{n-j}\sum_{t=1}^{n-j} x_t^* x_{t+j}^*$, and $R_{yy}(j) = \frac{1}{n-j}\sum_{t=1}^{n-j} y_t^* y_{t+j}^*$. The asterisk denotes the standardization for a variable, j is the lead/lag time steps, and t is time. The impact of ENSO on the stratosphere likely do not interfere with our composites, because the composite winter-mean Niño3.4 is approximately zero in reanalyses and most CMIP5/6 models (except CMCC-CMS and CESM2-WACCM).

To better compare the fine structure of the QBO in CMIP5/6 models with reanalyses, the phase-angle technique is also used in this study. The QBO cycle is divided into eight phases based on the 5-month running mean QBO30 index, which is fairly similar to the EEMD mode 4 of the original QBO30 (Huang et al. 2012; Hu et al. 2012). Huang et al. (2012) also reveal that the composite evolution of QBO cycle based on the smoothed QBO30 and $d\mathrm{QBO30}/dt$ is consistent with the composite evolution based on the EOF1 and EOF2 of equatorial zonal winds. Therefore, we only show the composite in a phase-angle space determined by QBO30 and its time tendency for succinctness. The procedures for classification of eight QBO phases are as follow.

Accepted for publication in *Journal of Climate*. DOI10.1175/JCLI-D-19-0663.1.

1. Choose the zonal mean zonal wind at 30hPa as the QBO index (QBO30).
2. Calculate the monthly tendency of QBO30 using the centered finite difference.
3. Calculate the phase angle tangent, $\tan\varphi = \frac{\mathrm{normalized(QBO30)}}{\mathrm{normalized\ (dQBO30/dt)}}$.
4. Calculate the phase angle from its tangent value and the signs of QBO30 and $d\mathrm{QBO30}/dt$. Modify the phase angle to fall into the value range (–π, π],

$$\varphi = \begin{cases} \arctan\left[\frac{\mathrm{normalized(QBO30)}}{\mathrm{normalized\ (}d\mathrm{QBO30/dt)}}\right], & \frac{\mathrm{dQBO30}}{dt} < 0 \\ \arctan\left[\frac{\mathrm{normalized(QBO30)}}{\mathrm{normalized\ (}d\mathrm{QBO30}/dt)}\right] - \pi, & \frac{d\mathrm{QBO30}}{dt} \geq 0 \text{ and } \mathrm{QBO30} > 0 \\ \arctan\left[\frac{\mathrm{normalized(QBO30)}}{\mathrm{normalized\ (}d\mathrm{QBO30}/dt)}\right] + \pi, & \frac{d\mathrm{QBO30}}{dt} \geq 0 \text{ and } \mathrm{QBO30} < 0 \end{cases}.$$

5. Split the QBO30 into phases 1–8 according to the phase angle range: (–π, –0.75π]; (–0.75π, –0.5π]; (–0.5π, –0.25π]; (–0.25π, 0]; (0, 0.25π]; (0.25π, 0.5π]; (0.5π, 0.75π]; (0.75π, π].

Because the composite circulation during two phase angles, φ and $\varphi + \pi$, are generally antisymmetric, we will only show the composite difference between phases 5–8 (QBO easterlies) and phases 1–4 (QBO westerlies) later (e.g., Anstey et al. 2010). In order to form a continuous timeseries of QBO evolution, the data in all months are used to define the QBO phase, but we then only select wintertime (November–March) data when studying the HT effect. To better understand the extratropical planetary wave response, the Eliassen-Palm (E-P) flux (F_y, F_z) and its divergence are diagnosed for models (Andrews et al. 1987). The residual stream function is also calculated for all models by integrating the residual meridional or vertical velocity ($\bar{v}^*, \bar{w}^*$) deduced from the transformed Eulerian-mean equation (Andrews et al. 1987; Garfinkel and Hartmann 2011a; Rao et al. 2019a).

3. Representation of QBO in CMIP5/6 models

The pressure-time evolution of the equatorial zonal winds from 200–5hPa are shown in Fig. 1 for the ERA-Interim and JRA55 reanalyses, as well as seven CMIP5 models and nine CMIP6 models. The evolutions of QBO in ERA-Interim and JRA55 are nearly identical with the

Accepted for publication in *Journal of Climate*. DOI10.1175/JCLI-D-19-0663.1.

easterly amplitude much stronger than the westerly amplitude (Figs. 1a, 1b). Although the QBO in CESM1-WACCM is nudged toward the observation, the tropical westerly and easterly amplitudes are much more symmetric than in the reanalyses (Fig. 1c). The QBO in all other models is generated spontaneously, with different degrees of fidelity (Figs. 1d–1r). Some QBO cycles in CMCC-CMS are irregular: westerlies in the upper stratosphere and easterlies in the middle stratosphere exhibit a prolonged stalling behavior between model years 1–6 (Fig. 1d). All models show a downward descent of the QBO from the upper to lower stratosphere. The QBO westerlies in 6 CMIP6 models are largely underestimated (Figs. 1j–1n, 1p), and they only develop in the mid-to-upper stratosphere. In contrast, the QBO is better simulated in GEOSCCM, HadGEM2-CCS, MIROC-ESM-CHEM, MIROC-ESM, MPI-ESM-MR, IPSL-CM6A-LR, MRI-ESM2-0 (Figs. 1e, 1f–1i, 1o, 1q). The asymmetry between relatively stronger easterlies and weaker westerlies are also reproduced in those models. The cycle of the QBO, especially its easterly phase in UKESM1-0-LL, is much longer than in reanalyses (4 cycles/13 years vs 5 cycles/13 years).

To better quantify the periodicity of the QBO in CMIP models, Fig. 2 shows the spectral analysis on the QBO30 from each dataset with the peak period highlighted by a vertical line. It is shown that the peak period is around 28 months in reanalyses (Figs. 2a, 2b), consistent with the dominant QBO period reported in early studies (e.g., Naujokat 1986; Baldwin et al. 2001). The QBO period in seven models is shorter than that in reanalyses, indicating a faster downward descent of QBO winds in those models (Figs. 2d, 2e, 2h, 2j, 2l–2n). In contrast, the range of the QBO period in eight models is similar to reanalyses (Figs. 2c, 2f, 2g, 2i, 2k, 2o–2q), and it should be noted that the QBO in CESM1-WACCM (Fig. 2c) is nudged toward observations. However, the QBO period in UKESM1-0-LL (Fig. 2r) is much longer than in reanalyses, corresponding to a slower downward propagation of QBO winds from the upper stratosphere to lower stratosphere (4.5 or 4 cycles in 13 years; Fig. 1r). In addition to the QBO

Accepted for publication in *Journal of Climate*. DOI10.1175/JCLI-D-19-0663.1.

peak period varying between models, the significant QBO period width is also not exactly identical. Based on reanalyses (Figs. 2a, 2b), the QBO period width is around 20–36 months, well simulated in most models. However, the period band is much narrower in MIROC-ESM-CHEM, MIROC-ESM, CNRM-CM6-1, CNRM-ESM2-1, and EC-Earth3, but wider in UKESM1-0-LL (Figs. 2g, 2h, 2l–2n, 2r).

4. Seasonality of the HT relationship in CMIP5/6 models

4.1 The HT relationship in early winter

The high latitude impact of QBO was reviewed in Anstey and Shepherd (2014), and the maximum NH extratropical response to QBO occurs in early winter (see their Fig. 3). The composite difference in early winter (November–January) between EQBO and WQBO events (their sample sizes shown in Table 2) for zonal mean zonal winds, scaled E-P flux, and E-P flux divergence is shown in Fig. 3. The composite difference pattern is largely similar between ERA-Interim and JRA55, and the composite zonal winds are more significant in JRA55 than ERA-Interim due the larger sample size in JRA55 (1958–) than ERA-Interim (1979–). As the QBO winters are selected using the QBO30 index, the maximum composite easterlies are situated at 30 hPa, with westerlies above 7 hPa in reanalyses (Figs. 3a, 3b). It can be seen from reanalyses that a significant E-P flux divergence dipole is established between 20–50°N, 30–5hPa and 50–80°N, 100–5hPa in early winter, corresponding to a strong poleward propagation of planetary waves between the two dipole centers. The E-P flux convergence center in the circumpolar region indicates dissipation of waves there and explains the easterly response. The E-P flux divergence dipole is driven largely by poleward propagation of waves, while the upward propagation of waves in mid-to-upper stratosphere over the Arctic is a minor contributor, although some anomalous wave propagation in the upper troposphere and lowermost stratosphere is also apparent. Not all models can reproduce the circumpolar easterly response pattern. For example, the easterly response at high latitudes in CESM1-WACCM is

Accepted for publication in *Journal of Climate*. DOI10.1175/JCLI-D-19-0663.1.

biased upward to much lower pressure levels (Fig. 3c), while westerly response appears at mid–high latitudes for MRI-ESM2-0 (Fig. 3q). The E-P flux divergence dipole can be simulated with different degrees of success in most models except BCC-CSM2-MR and MRI-ESM2-0 (Figs. 3j, 3q). The MRI-ESM2-0 output analyzed here is different from Naoe and Yoshida (2019): they used AMIP-type simulations but we use the historical run. Naoe and Yoshida (2019) found that the MRI-ESM2-0 shows an equatorward branch of the E-P flux anomalies in the midlatitude lower stratosphere, and that more waves in the midlatitude stratosphere propagate poleward, not clearly verified by the EQBO minus WQBO composite in Fig. 3q.

Although the poleward propagation of waves from midlatitudes in the stratosphere is partially responsible for the weakening of the polar vortex in reanalyses, the E-P flux response varies with models. The E-P flux diverges in midlatitudes and converges at high-latitudes in 10 models (Figs. 3d, 3e, 3g, 3h, 3k–3o, 3r). Such poleward E-P flux response is biased to lower pressure levels in CESM1-WACCM (Fig. 3c), reversed in HadGEM2-CCS (Fig. 3f), not as apparent as upward E-P flux in MPI-ESM-MR, BCC-CSM2-MR, and MIROC6 (Figs. 3i, 3j, 3p), and not realistically reproduced in MRI-ESM2-0 (Fig. 3q). Therefore, the HT mechanism might not be enough to explain the equatorward branch of the E-P flux anomalies, as in all models examined here the zero-wind line is modified by the QBO but the E-P flux anomalies are less consistent.

4.2 Direct response of the meridional circulation in early winter

To better understand the zonal wind anomalies, the composite temperature and residual velocity ($\bar{v}^*$, $\bar{w}^*$) anomalies in early winter are shown in Fig. 4 for reanalyses and CMIP5/6 models. Based on reanalyses (Figs. 4a, 4b), it is observed that over the equator the cold temperature and positive $\bar{w}^*$ (upwelling) anomalies appear below the maximum easterlies center (~30 hPa) to balance the easterlies increasing with height (i.e., $-\frac{\partial \bar{u}}{\partial z} > 0$ corresponds to $-\frac{\partial^2 \bar{T}}{\partial y^2} < 0$ by thermal wind balance), whereas warm temperature and negative $\bar{w}^*$

Accepted for publication in *Journal of Climate*. DOI10.1175/JCLI-D-19-0663.1.

(downwelling) anomalies prevail above the maximum easterlies center to balance the easterlies decreasing with height (i.e., $-\frac{\partial \bar{u}}{\partial z} < 0$ corresponds to $-\frac{\partial^2 \bar{T}}{\partial y^2} > 0$; see Eq. 8.2.2 in Andrews et al. 1987, P318). In contrast, the downwelling in the equatorial upper stratosphere is much stronger than the upwelling in the equatorial lower stratosphere, and it is coupled with the extratropical upwelling. The extratropical upwelling can well explain the local cold anomalies. The coupled upwelling in the tropics and downwelling in the extratropics directly induced by the QBO through the thermal wind balance are part of an anticlockwise circulation cell. Similarly, a clockwise circulation cell is excited in the lower stratosphere and upper troposphere, corresponding to the lower stratospheric temperature dipole, i.e., cold tropics and warm extratropics. The meridional circulation cell, and in particular the residual vertical and meridional velocities, modifies the distribution of zonal momentum and explains the downward and poleward arching of westerlies and easterlies in a horseshoe-like shape in the subtropics (e.g., Randel et al. 1999; Garfinkel and Hartmann 2011a, 2011b; Coy et al. 2016). The anomalous upwelling in the midlatitude stratosphere is split into an equatorward branch descending into the tropical upper stratosphere and a poleward branch descending in the polar region and inducing warm anomalies.

The enhanced downwelling in the Arctic stratosphere and the warm response through adiabatic heating is better simulated in CMCC-CMS, GEOSCCM, HadGEM2-CCS, MIROC-ESM, MPI-ESM-MR, BCC-CSM2-MR, CESM2-WACCM, CNRM-CM6-1, CNRM-ESM2-1, MIROC6, and UKESM1-0-LL (Figs. 4d–4f, 4h–4m, 4p, 4r) than other models. Consistent with Fig. 3, the polar downwelling and warm response are biased upward to lower pressure levels in CESM1-WACCM, MIROC-ESM-CHEM, EC-Earth3, IPSL-CM6A-LR, and MRI-ESM2-0 (Figs. 4c, 4g, 4n, 4o, 4q). Although most CMIP5/6 models can well capture the warm and weak stratospheric polar vortex response during EQBO winters, the warm temperature response amplitude in models tends to be underestimated, which is mainly caused by the

Accepted for publication in *Journal of Climate*. DOI10.1175/JCLI-D-19-0663.1.

weaker wave activities in the extratropics (Fig. 3) in models. The residual circulation is mainly driven by wave activities of different scales, but we only calculate the contribution by planetary waves diagnosed with monthly data for GEOSCCM (daily data for reanalyses and other models) due to the unavailability of daily outputs for this model. Note that Garfinkel et al. (2012) demonstrate that it is mainly stationary planetary waves that lead to the HT effect.

4.3 Stratospheric polar vortex and surface

To better assess the performance of CMIP5/6 models in simulating the HT relationship in early and late winter, several indicators are calculated, including the polar mean sea level pressure ($MSLP_{pole}$; averaged over 60–90°N), the lower stratospheric temperature over the Arctic ($T_{pole/200–50hPa}$; averaged over 60–90°N, 200–50hPa), E-P flux divergence in the circumpolar stratosphere ($divEP_{60–80°N/100–10hPa}$; averaged over 60–80°N, 100–10hPa), the E-P flux divergence dipole between 60–80°N, 100–10hPa and 30–50°N, 30–10hPa, and stratospheric downwelling over the Arctic ($\overline{w}^{*}_{65-85°N/100-10hPa}$, averaged over 65–85°N, 100–10hPa). The model-by-model scatterplots of $MSLP_{pole}$ vs $T_{pole/200–50hPa}$, $divEP_{60–80°N/100–10hPa}$ vs $T_{pole/200–50hPa}$, and E-P divergence/convergence dipole vs $\overline{w}^{*}_{65-85°N/100-10hPa}$ are shown in Fig. 5. On average, a weak and warm polar vortex is seen in early winter (November–January, purple markers) during EQBO from reanalyses (open purple squares, # 1 and 2), which is projected onto the negative NAM propagating downward. Therefore, positive $MSLP_{pole}$ anomalies are observed in early winter and persist into late winter (open green squares). The stratospheric pathway linking EQBO and the extratropical surface response, i.e., negative AO denoted by positive $MSLP_{pole}$ anomalies can be reproduced by three models, nos. 6, 8, and 16 in Fig. 5a (i.e., HadGEM2-CCS, MIROC-ESM, and MIROC6), although positive $T_{pole/200–50hPa}$ anomalies are simulated in most models. Over the multi-model ensemble (MME), the polar stratospheric temperature is positively correlated with the polar MSLP, although at a low confidence level (α=0.06). Therefore, the underestimated stratospheric polar vortex response

Accepted for publication in *Journal of Climate*. DOI10.1175/JCLI-D-19-0663.1.

to QBO is partially responsible for the weak $MSLP_{pole}$ anomalies in most models in both early (November–January) and late (February–March) winter.

The small stratospheric polar vortex response amplitude or the underestimated HT relationship in most models is related to the smaller-than-observed November–January E-P flux convergence anomalies in the circumpolar stratosphere (Fig. 5b) or the E-P flux divergence dipole between mid- and high latitudes (not shown). The E-P flux convergence anomalies (i.e., divEP < 0) in early winter during EQBO for reanalyses and most models (see the second quadrant in Fig. 5b) correspond to more dissipation of planetary waves in the polar stratosphere, whereas there is weaker upward wave propagation in late winter as the stratosphere polar vortex is already weakened and gradually recovers after February in reanalyses. However, the timing of the HT relationship within the extended winter is incorrect for several models: The E-P flux convergence anomalies in the polar stratosphere and positive polar cap temperature anomalies are strongest in early winter for reanalyses, but they are strongest in late winter for some models (e.g., CMCC-CMS and CNRM-ESM2-1).

Strong wave dissipation in the polar stratosphere (divEP < 0) is dynamically related to the anomalous downwelling ($\overline{w}^* < 0$) over the Arctic in early winter during EQBO, whereas the dynamical downwelling response largely diminishes as the polar vortex recovers in late winter (see open squares in Fig. 5c). Most models can reproduce the dynamical downwelling in early winter during EQBO except HadGEM2-CCS (#6). The maximum downwelling response in HadGEM2-CCS is delayed to late winter associated with the strong E-P flux divergence dipole. The seasonal locking of the polar downwelling is not seen in CMIP5/6 models: The anomalous downwelling is still present until late winter in models, whereas it has already disappeared in reanalyses. It is still difficult for CMIP5/6 models to reproduce the polar vortex response varying with season, and the positive relationship between the polar downwelling and the E-P flux convergence through "downward control" is also fairly weak between models. Despite

Accepted for publication in *Journal of Climate*. DOI10.1175/JCLI-D-19-0663.1.

those biases, the early-winter downwelling response in the polar stratosphere associated with dissipation of waves originating from midlatitudes (divEP > 0) to high latitudes (divEP < 0) is successfully captured by most models.

5. Evaluation of QBO-stratospheric polar vortex relationship based on the QBO phase-angle space

5.1 Composite QBO cycle from phase 1 to phase 8

The composite EQBO minus WQBO difference from reanalyses shows the strongest extratropical response in early winter, whereas such a seasonality is not present in most models. The composite QBO structure in Fig. 3 is somewhat different between reanalyses and models, the westerlies above the easterlies at the equator develop higher in reanalyses (above 7 hPa) than models (above 10hPa). The dependence of the extratropical response to the QBO structure is investigated in this section.

The composite evolutions of the equatorial zonal wind anomalies with the QBO phase from 200–5hPa are shown in Fig. 6 for reanalyses and models. Given that the QBO phases are defined using the QBO30 index, phase 1 (5) corresponds to the 30-hPa westerly (easterly) initiating stage when the westerlies (easterlies) centered between 20hPa and 10hPa begin to descend. Similarly, phase 2 (6) is the 30-hPa westerly (easterly) developing stage, phase 3 (7) is the westerly (easterly) weakening stage, and phase 4 (8) is the westerly (easterly) decaying stage. Phase 9 in Fig. 6 is a replication of phase 1, included for visualization only. The QBO exhibits a twofold structure between 200–5 hPa (i.e., westerlies overlying easterlies during phases 1–4; vice versa during phases 5–8), and often a threefold structure (i.e., a third anomaly center above 5hPa in the upper stratosphere, not shown) (Pascoe et al. 2005).

The downward propagation of westerlies (easterlies) from phase 6 (2) at 5hPa to the following phase 5 (1) above 100hPa in reanalyses (Figs. 6a, 6b) is well simulated in CMIP5/6 models (Figs. 6c–6r). The main bias is the unrealistic QBO wind amplitude in some models:

Accepted for publication in *Journal of Climate*. DOI10.1175/JCLI-D-19-0663.1.

The composite QBO winds in seven CMIP6 models (Figs. 6j–6p) are underestimated, consistent with the early-winter composites (Figs. 3j–3p).

5.2 Varying extratropical response with the QBO evolution

Next, we explore the stratospheric polar vortex state during the eight QBO phases in November–March, denoted by the composite polar cap temperature (averaged over 60–90°N) and circumpolar zonal wind (averaged over 55–75°N) anomalies. The evolution of the polar cap temperature and zonal wind anomalies with the QBO phase from 1000–5hPa are shown in Fig. 7. Due to the small sample size in ERA-Interim, it is easy to understand that the composite anomalies from ERA-Interim are less significant than those from JRA55 and models. It can be seen that the varying polar response with the QBO phase is well simulated in all models, showing a downward propagation. The cold lower stratospheric polar vortex and accelerated polar night jet are observed during QBO phases 2–4, whereas the warm stratospheric polar vortex and decelerated polar night jet occur during QBO phases 6–8 (Figs. 7a, 7b), which is successfully modelled by all CMIP5/6 models (Figs. 7c–7r). The maximum lower stratospheric temperature anomalies over the polar cap appear during the phases 3 and 7, although the circumpolar zonal wind anomalies reach maxima later. Warm (Cold) anomalies first appear during phase 4 (8) above 5hPa and descend to the troposphere during phase 6 (2). All models show high sensitivity of the polar cap temperature and circumpolar wind response to the QBO phase, consistent with reanalyses. Due to the much shorter data record, the weakened significance and weak anomalies in ERA-Interim as compared to JRA55 and the models might mainly reflect internal variability.

The composite differences of zonal winds, E-P flux, and E-P flux divergence between the QBO phase 7 and phase 3 during the extended winter (November–March) are shown in Fig. 8 for reanalyses and all CMIP5/6 models. Compared with the composite difference between EQBO and WQBO in Fig. 3 (i.e., EQBO minus WQBO), the extratropical response to QBO

Accepted for publication in *Journal of Climate*. DOI10.1175/JCLI-D-19-0663.1.

(i.e., phase 7 minus phase 3) in Fig. 8 is more organized and reproduced by all models. In other words, the extratropical response during each of the eight QBO phases is much stronger than the seasonal (early or late winter) EQBO minus WQBO composite, especially in models. Due to the large variability in the stratosphere and small sample size in ERA-Interim (<40 years), the composite wind response in the polar stratosphere is nonsignificant at the 95% confidence level (Fig. 8a). However, the extratropical response patterns are fairly similar for all CMIP5/6 models. Specifically, the E-P flux divergence dipole, especially its convergence center in the polar stratosphere, is seen in all models except that the anomaly amplitude in MIROC6 is somewhat underestimated (Fig. 8p). Waves tend to propagate towards high refractive index (not shown; see Garfinkel et al. 2012), explaining the midlatitude stratospheric E-P flux divergence and more waves dissipating in the polar upper stratosphere. In contrast, the E-P flux divergence dipole for the phase 7 minus phase 3 difference is much better simulated by CESM1-WACCM, MIROC-ESM-CHEM, MIROC-ESM, CNRM-CM6-1, CNRM-ESM2-1, IPSL-CM6A-L, MRI-ESM2-0, and UKESM1-0-LL (Figs. 8c, 8g, 8h, 8l, 8m, 8o, 8q, 8r) than other models. Those eight models are dominated by poleward E-P flux in the extratropical upper stratosphere, but the upward-propagating waves from the troposphere are also modelled in the polar stratosphere. However, upward-propagating planetary waves are stronger than poleward-propagating waves in the upper stratosphere in some remaining models (Figs. 8d, 8e, 8i, 8j).

In order to better understand the wave response in Fig. 8, the maximum temperature response in the Arctic stratosphere throughout the QBO lifecycle is shown in Fig. 9, denoted as the difference between phase 7 and phase 3. Comparing Figs. 9 and 4, it is shown once again that the distinction of the stratospheric polar vortex response between early and late winter is related to the QBO phases for most models. All models reveal that the stratospheric polar vortex is anomalously warm associated with the polar adiabatic heating by anomalous

Accepted for publication in *Journal of Climate*. DOI 10.1175/JCLI-D-19-0663.1.

downwelling. The direct meridional circulation response in the upper stratosphere is identified in all models, that is, upwelling in midlatitudes and dowelling in the equatorial and polar regions. Associated with the midlatitude upwelling, significant cold anomalies form in the extratropical upper stratosphere (Figs. 9a, 9b), which are underestimated by at least four CMIP6 models, obscured by warm anomalies centered at the equator (Figs. 9k–9m, 9o). Similarly, associated with the clockwise circulation cell across tropical–subtropical mid-to-lower stratosphere, a pattern of cold tropics–warm subtropics is seen in reanalyses (Figs. 9a, 9b). It is clear that the cold center in the tropical mid-to-lower stratosphere is simulated in all models, but the warm center in the subtropical mid-to-lower stratosphere is largely underestimated and/or biased upward in eight models (Figs. 9d–9i, 9o, 9p). In contrast, such a warm center even disappears in five CMIP6 models (Figs. 9j–9n). The subtropical warm center in the lower stratosphere underneath a cold center in the upper stratosphere is relatively better simulated by three models, i.e., CESM1-WACCM, MRI-ESM2-0, UKESM1-0-LL (Figs. 9c, 9q, 9r).

5.3 QBO's stratospheric pathway for the extratropical response

Through the HT mechanism during the EQBO, the weakened stratospheric polar vortex is usually projected onto the negative NAM and corresponds to a negative surface AO (Gray et al. 2018). Therefore, the stratospheric pathway is of vital importance in linking the QBO and troposphere or near surface. The scatterplot of polar MSLP anomalies is shown in Fig. 10a for all composite differences (phases 5–1, 6–2, 7–3, and 8–4) during the extended winter (November–March) from all datasets. The scatter points ($MSLP_{pole}$ vs $T_{pole/200–50hPa}$) for phases 7–3 tend to situate in the top right, indicating the positive $MSLP_{pole}$ and $T_{pole/200–50hPa}$ anomalies for phases 7–3 are stronger than for phases 5–1 and phases 6–2. It is also shown that the composite MSLP difference for phases 8–4 is comparable to that for phases 7–3, although the

Accepted for publication in *Journal of Climate*. DOI10.1175/JCLI-D-19-0663.1.

$T_{\mathrm{pole/200–50hPa}}$ anomalies for phase 8–4 have diminished. This indicates that the maximum surface QBO signal lags the maximum stratospheric QBO response in its phase for models and reanalyses. The positive correlation between $T_{\mathrm{pole/200–50hPa}}$ and $\mathrm{MSLP}_{\mathrm{pole}}$ suggests that the stratospheric polar vortex can act as the medium communicating the QBO influence downward to near surface.

Similar to Fig. 4b, the relationship between $T_{\mathrm{pole/200–50hPa}}$ and the E-P flux divergence in the polar stratosphere is shown in Fig. 10b for the composite difference from models and reanalyses between phases 5-to-8 and 1-to-4, respectively. The model-by-model points in Fig. 10b are fairly concentrated for the difference between each pair of phases (i.e., phases 5–1, 6–2, 7–3, and 8–4) but are very scattered in total. The correlation between polar lower stratospheric temperature and E-P flux divergence is calculated separately for each pair of phases with 180° lag/lead. The negative correlation for phases 5–1, 6–2, and 7–3 confirms that the intensity of the polar vortex is closely associated with dissipation of waves in the polar stratosphere, which mainly originate from the lower-latitude stratosphere and partly the troposphere. However, the modelled $T_{\mathrm{pole/200–50hPa}}$ and the E-P flux divergence differences between phases 8 and 4 show similar amplitudes in most models, and their correlation is much weaker than in other phases. When the polar vortex is disturbed, the wave dissipation into the polar stratosphere gradually weakens and then disappears from phase 6, phase 7 to phase 8 (i.e., the scatter group shifts rightward from green, orange to red).

The E-P flux divergence dipole between midlatitude and polar stratosphere can quantify the anomalous wave source directly associated with QBO in the mid-to-upper stratosphere, which modulate the residual circulation. The model-by-model scatter plot of polar stratospheric downwelling vs the E-P flux divergence dipole is shown in Fig. 10c for each pair of phases with 180° lead/lag. The poleward-propagating waves dissipating in the circumpolar stratosphere are obvious in phases 7 and 8 in reanalyses, but they form at the beginning of the

Accepted for publication in *Journal of Climate*. DOI10.1175/JCLI-D-19-0663.1.

QBO winds reversal to easterlies (i.e., phase 5) in most models, persist until phase 7, and then disappear early during phase 8.

6. A possible reason for the seasonal drift of the modelled HT relationship

Based on the evaluation of extratropical response to each of eight QBO phases in the last section, it is shown that the CMIP5/6 models can successfully reproduce (and may even exaggerate) the stratospheric response during phases 7 and 3 if the full extended winter (November–March) is examined. In contrast, section 4 showed that if one focuses on the early-winter only, the large difference between EQBO and WQBO in reanalyses is not captured by the models, and rather the significant stratospheric polar response in some models shifts to late winter. Does this divergence between the models and observations in the timing of the peak HT effect reflect a model bias? Or does it reflect a difference in the frequency of occurrence of specific QBO phases over the course of the extended winter?

We now assess whether there is any relationship between the seasonal drift of the HT relationship and the Probability Distribution Function (PDF) of eight QBO phases in models. We specifically show that the maximum extratropical response to QBO in early winter in observations is simply caused by the higher PDF of phases 7 and 3 in early winter months, but no such tendency is evident for the models. To explain the seasonal locking of the HT relationship to early winter in reanalyses, the PDF of the QBO30 phases are shown in Fig. 11 for 2 reanalyses and 16 CMIP5/6 models. It is indeed shown that the two-dimensional PDF value as a function of month and the QBO phase from reanalyses (Figs. 11a, 11b) is largest near the QBO phase 3 during August–January (late summer–early winter). However, the phase 3 shows a much smaller possibility of appearing in February–July. It is unclear whether this tendency of QBO phase 3 to occur in early winter reflects a forced response of the QBO to the seasonal cycle, or may have occurred by chance in the relatively short observational record. Similarly, the probability density in phase 7 is also much larger especially during November

Accepted for publication in *Journal of Climate*. DOI10.1175/JCLI-D-19-0663.1.

than during late winter months (Figs. 11a, 11b). Because the QBO cycle might shorten in a warmer future earth with its amplitude weakened (Kawatani and Hamilton 2013; Schirber et al. 2014), one may expect that the PDF of QBO as a function of its phase and month will become much more uniform if the sample size is large enough in the future.

In contrast, the PDF of QBO in models and the multimodel ensemble is much more uniform than in reanalyses, likely due to the much longer timespan in the historical run (Figs. 11c–11s). Most models with a relatively stronger stratospheric anomaly over the Arctic in early winter (Figs. 3 and 4) show a higher PDF at phases 3–4 or/and 7–8 in late summer–early winter months than in later winter months (Figs. 11d, 11h–11j, 11l, 11m, 11p, 11r). Some previous studies emphasized the importance of the annual cycle for the impact of QBO on the extratropics (Anstey and Shepherd 2008; Anstey et al., 2010; Rajendran et al. 2016, 2018), but the QBO evolution stage might play a more dominant role for the extratropical response pattern. The seasonal shift of the maximum polar response to late winter in several models (Fig. 5) might provide modelling evidence that the QBO tendency should also be considered in empirical prediction models.

7. Summary and discussion

This study uses the state-of-the-art CMIP5/6 models with QBO-like cycles in the equatorial stratosphere to assess the relationship between the QBO and the northern winter stratospheric polar vortex (the HT effect). The observed maximum HT relationship in early winter from reanalyses is also compared among CMIP5/6 models, and the AO-like response denoted by the polar MSLP anomaly is evaluated for CMIP models in early and late winter. In addition, the extratropical response to eight QBO30 phases are also reported, and dynamics are diagnosed. The main findings in our paper are as follow.

Compared with CMIP5, more CMIP6 models can reproduce the QBO-like phenomenon, although the QBO period in models is not exactly the same as in reanalyses. Based on the

Accepted for publication in *Journal of Climate*. DOI10.1175/JCLI-D-19-0663.1.

spectrum analysis on the QBO30 index in different datasets, the dominant period of the 30-hPa equatorial zonal winds in two reanalyses (ERA-Interim and JRA55) is ~28 months. Eight models (e.g., CESM1-WACCM, HadGEM2-CCS, MIROC-ESM-CHEM, MPI-ESM-MR, CESM2-WACCM, IPSL-CM6A-LR, MIROC6, MRI-ESM2-0) can well simulate the dominant QBO period ranging from 25 to 31 months. In contrast, seven models (i.e., CMCC-CMS, GEOSCCM, MIROC-ESM, BCC-CSM2-MR, CNRM-CM6-1, CNRM-ESM2-1, EC-Earth3) show a somewhat faster QBO period but UKESM1-0-LL shows a much slower QBO.

The HT relationship in early winter is simulated in most CMIP5/6 models, that is, the circumpolar westerlies are decelerated and the stratospheric polar cap is anomalously warm during EQBO; vice versa during WQBO. The downward and poleward arching of the maximum easterlies during EQBO reported in early studies (Garfinkel and Hartmann 2011a, 2011b; Garfinkel et al. 2012; White et al. 2015, 2016) is identified in CMIP5/6 models, which indeed drives the zero-wind line in the subtropical upper troposphere further poleward (Holton and Tan 1980; Rao et al. 2019a and reference therein). The westerlies above the maximum easterlies also arch downward and poleward but into the midlatitude stratosphere, corresponding to an E-P flux divergence center there. The net effect is (1) that more waves in the mid-to-upper stratosphere propagate poleward and (2) that upward wave propagation in the subpolar lower stratosphere is enhanced. Therefore, an anomalous E-P flux convergence center forms in the polar region, which is simulated by all CMIP5/6 models. However, a few models (e.g., MPI-ESM-MR, BCC-CSM2-MR, and MIROC6) only emphasize the contribution of upward-propagating waves from the troposphere but underestimate the poleward E-P flux emitting from the midlatitude upper stratosphere. Namely, the HT mechanism can well explain the polar response in the lower stratosphere, but the polar response in the upper stratosphere is even stronger due to wave dissipation of poleward-propagating waves denoted by an E-P flux divergence dipole. The wave response in the upper stratosphere is related to changes in the

Accepted for publication in *Journal of Climate*. DOI10.1175/JCLI-D-19-0663.1.

background circulation through the meridional-vertical circulation cells directly excited by the QBO. All models and reanalyses consistently show an anomalous anticlockwise circulation cell in lower latitudes above the maximum EQBO wind center, and the midlatitude upwelling is split into two branches, one of which goes northward and descends in the Arctic region and warms the stratospheric polar vortex through adiabatic heating associated with downwelling. In contrast, a relatively weak and shallow clockwise circulation cell forms in the lower stratosphere at lower latitudes. Most models can well capture the Arctic stratospheric warming in early winter during EQBO, although the response amplitudes are somewhat weaker in some models (e.g., CESM1-WACCM, GEOSCCM, HadESM2-CC, MIROC-ESM-CHEM, EC-Earth3, IPSL-CM5A-LR, MRI-ESM2-0).

The QBO can affect near surface climate by modulating the stratospheric polar vortex variations, which project onto the NAM propagating downward to influence the surface AO. Such a route was established by previous studies (e.g., Baldwin and Dunkerton 1998; Thompson and Wallace 2000; Garfinkel et al. 2012) and verified in this study by checking the relationship between $\mathrm{MSLP}_{\mathrm{pole}}$ and $T_{\mathrm{pole/200–50hPa}}$, although their correlation is at a relatively low confidence level (α=0.2) based on the early winter composite. Further, the underestimated polar warm anomalies in models during EQBO are linked to the weaker-than-observed wave dissipations (i.e., E-P flux convergence anomalies). However, the polar downwelling during EQBO and its relationship with the wave driving are not well reproduced in models. Some models have a seasonal drift of the observed maximum HT relationship in early winter to late winter.

To stress the importance of the QBO phase for the extratropical response, we also divide the QBO into eight phases based on the QBO30 index and its tendency. Based on the composite QBO cycle, it is revealed that the average QBO amplitude in several models (i.e., CMCC-CMS, MIROC-ESM, BCC-CSM2-MR, CESM2-WACCM, CNRM-CM6-1, CNRM-ESM2-1, EC-

Accepted for publication in *Journal of Climate*. DOI10.1175/JCLI-D-19-0663.1.

Earth3, MIROC6) are largely underestimated. According to the phase-based composite, a regular cycle of the extratropical response is identified in all models and reanalyses. The maximum warm (cold) polar stratosphere is found during the QBO phase 7 (3). As the QBO cycle evolves, the stratospheric anomalies first appear in the upper stratosphere and descend gradually into the troposphere. Compared with the early winter composite (EQBO minus WQBO), the phase-based composite (phase 7 minus 3) is much more organized and stronger in models, which might indicate the dependence of extratropical QBO signal on the equatorial QBO phase rather than the month. In addition, negative surface AO-like pattern forms during the QBO phase 7; and vice versa during the QBO phase 3.

By using the phase-based composite, it is revealed that the negative surface AO response in models is positively correlated with the weakening of the stratospheric polar vortex. The stratospheric polar vortex state, in turn, is associated with total wave dissipation into the polar region. The E-P flux divergence dipole in the upper stratosphere is not only an indicator of enhanced poleward-propagating waves (or weakened equatorward-propagating waves), but also an indicator of polar downwelling, which is not clearly established by the EQBO minus WQBO composite during early winter. The net effect is that while seasonal dependence of the HT relationship differs between the models and reanalyses, the response to a given QBO phase (taking all months in the extended winter, November–March) is similar in models and observations. The maximum HT relationship observed in early winter might be caused by the configuration of the QBO phases 7 and 3 with early winter months in observations, a tendency that is not evident in the models. The observed seasonality of QBO's impact on the extratropics has already been documented (Anstey et al. 2010; Rajendran et al. 2016, 2018). Anstey et al. (2010) used ERA40 reanalysis and CMAM (Canadian Middle Atmosphere Model) integrations to show that the strength and timing of QBO influence on the vortex may be affected by the seasonal synchronization of QBO phase transitions. In contrast, the PDF of the QBO phases is

Accepted for publication in *Journal of Climate*. DOI10.1175/JCLI-D-19-0663.1.

more uniform in models, possibly because the observed effect is a consequence of a relatively small sample size. This difference in the relative timing of QBO phases 7 and 3 in the annual cycle can explain why the models simulate an overly weak early winter HT relationship.

All the experiments used in this study are air-sea coupled historical runs, so the ENSO teleconnection in the stratosphere is included in those SST free-evolving experiments, but a large sample size in the historical runs can decrease the possibility of interference of ENSO signals with QBO signals (see Table 2 for the composite Niño3.4). By using a large multimodel ensemble with QBO spontaneously generated, it becomes possible to separate the relative contribution of QBO and ENSO to the stratospheric variability, although the combined impact of ENSO and QBO on the stratospheric polar vortex was observed to be nonlinear about their intensity and phases (e.g., Garfinkel and Hartmann 2007; Calvo et al. 2009).

The CMIP6 database is still being populated, and it is likely that the number of models that simulate a QBO will grow. However, the 16 models examined here allow us an unprecedented dataset with several hundred easterly and westerly QBO events. While it will be worth revisiting the conclusions of this study in a few years after the CMIP6 database is nearly full, the large sample size spread across many different models allow us to understand how the HT effect compares in models and in observations, and in particular to demonstrate that the QBO phase, and not the specific month within the winter season, is the dominant arbiter of the strength of the HT effect.

Acknowledgments

JR was funded by the National Natural Science Foundation of China (41705024) and the National Key R&D Program of China (2016YFA0602104). CIG and IW are funded by the Israel Science Foundation (1558/14) and the European Research Council starting grant under the European Union’s Horizon 2020 research and innovation programme (677756). We acknowledge the ESGF for providing historical runs from sixteen CMIP5/6 models

Accepted for publication in *Journal of Climate*. DOI10.1175/JCLI-D-19-0663.1.

(https://esgf-node.llnl.gov/projects/esgf-llnl/). The ERA-Interim reanalysis is available from the ECMWF (https://apps.ecmwf.int/datasets/data/interim-full-daily/levtype=pl/), and the JRA55 reanalysis can be downloaded using FTP (https://jra.kishou.go.jp/JRA-55/index_en.html).

References

Andrews, D. G., and M. E. McIntyre, 1976: Planetary waves in horizontal and vertical shear: the generalized Eliassen–Palm relation and the mean zonal acceleration. *J. Atmos. Sci.*, **33,** 2031–2048.

Andrews, D. G., J. R. Holton, and C. B. Leovy, 1987: *Middle Atmosphere Dynamics*. Academic Press, 489 pp.

Andrews, M. B., J. R. Knight, A. A. Scaife, Y. Lu, T. Wu, L. J. Gray, and V. Schenzinger, 2019: Observed and simulated teleconnections between the stratospheric quasi-biennial oscillation and northern hemisphere winter atmospheric circulation. *J. Geophys. Res. Atmos.*, **124,** 1219–1232. doi:10.1029/2018jd029368.

Anstey, J. A., J. F. Scinocca, and M. Keller, 2016: Simulating the QBO in an atmospheric general circulation model: Sensitivity to resolved and parameterized Forcing. *J. Atmos. Sci.*, 73, 1649–1665. doi: 10.1175/jas-d-15-0099.1.

Anstey, J. A., and T. G. Shepherd, 2008: Response of the northern stratospheric polar vortex to the seasonal alignment of QBO phase transitions. *Geophys. Res. Lett.*, **35**, L22810. doi: 10.1029/2008gl035721.

Anstey, J. A., and T. G. Shepherd, 2014: High-latitude influence of the quasi-biennial oscillation. *Quart. J. Roy. Meteor. Soc.*, **140,** 1–21. doi:10.1002/qj.2132.

Anstey, J. A., T. G. Shepherd, and J. F. Scinocca, 2010: Influence of the quasi-biennial oscillation on the extratropical winter stratosphere in an atmospheric general circulation model and in reanalysis data. *J. Atmos. Sci.*, **67,** 1402–1419. doi:10.1175/2009jas3292.1.

Accepted for publication in *Journal of Climate*. DOI 10.1175/JCLI-D-19-0663.1.

Baldwin, M. P., and Coauthors, 2001: The quasi-biennial oscillation. *Rev. Geophys.*, **39,** 179–229. doi:10.1029/1999rg000073.

Baldwin, M. P., and T. J. Dunkerton, 1998: Quasi-biennial modulation of the southern hemisphere stratospheric polar vortex. *Geophys. Res. Lett.*, **25,** 3343–3346. doi:10.1029/98gl02445.

Baldwin, M. P., and K. K. Tung, 1994: Extra-tropical QBO signals in angular momentum and wave forcing. *Geophys. Res. Lett.*, **21,** 2717–2720. doi:10.1029/94gl02119.

Bell, C. J., L. J. Gray, A. J. Charlton-Perez, M. M. Joshi, and A. A. Scaife, 2009: Stratospheric communication of El Niño teleconnections to European winter. *J. Climate*, **22,** 4083–4096. doi:10.1175/2009jcli2717.1.

Boville, B. A., and W. J. Randel, 1992: Equatorial waves in a stratospheric GCM: Effects of vertical resolution. *J. Atmos. Sci.,* **49**, 785–801.

Butchart, N., and Coauthors, 2018: Overview of experiment design and comparison of models participating in phase 1 of the SPARC Quasi-Biennial Oscillation initiative (QBOi). *Geosci. Model Dev.*, **11,** 1009–1032. doi:10.5194/gmd-11-1009-2018.

Calvo, N., M. A. Giorgetta, R. Garcia-Herrera, and E. Manzini, 2009: Nonlinearity of the combined warm ENSO and QBO effects on the Northern Hemisphere polar vortex in MAECHAM5 simulations. *J. Geophys. Res.*, **114,** D13109. doi:10.1029/2008jd011445.

Calvo, N., and Coauthors, 2017: Northern Hemisphere stratospheric pathway of different El Niño flavors in stratosphere-resolving CMIP5 models. *J. Climate,* **30,** 4351–4371. doi:10.1175/jcli-d-16-0132.1.

Camp, C. D., and K. K. Tung, 2007: The influence of the solar cycle and QBO on the late-winter stratospheric polar vortex. *J. Atmos. Sci.*, **64,** 1267–1283. doi:10.1175/jas3883.1.

Canziani, P. O., and J. R. Holton, 1998: Kelvin Waves and the quasi-biennial oscillation: An observational analysis. *J. Geophys. Res.*, **103,** 31509–31521. doi:10.1029/1998jd200021.

Accepted for publication in *Journal of Climate*. DOI10.1175/JCLI-D-19-0663.1.

Charlton-Perez, A. J., and Coauthors, 2013: On the lack of stratospheric dynamical variability in low-top versions of the CMIP5 models. *J. Geophys. Res. Atmos.,* **118**, 2494–2505. doi:10.1002/jgrd.50125.

Choi, W., W. B. Grant, J. H. Park, K. M. Lee, H. Lee, and J. M. Russell, 1998: Role of the quasi-biennial oscillation in the transport of aerosols from the tropical stratospheric reservoir to midlatitudes. *J. Geophys. Res.,* **103,** 6033–6042. doi:10.1029/97jd03118.

Claud, C., and P. Terray, 2007: Revisiting the possible links between the quasi-biennial oscillation and the Indian summer monsoon using NCEP R-2 and CMAP fields. *J. Climate*, **20**, 773–787. doi:10.1175/jcli4034.1.

Collimore, C. C., D. W. Martin, M. H. Hitchman, A. Huesmann, and D. E. Waliser, 2003: On the relationship between the QBO and tropical deep convection. *J. Climate*, **16**, 2552–2568.

Davini, P., C. Cagnazzo, P. G. Fogli, E. Manzini, S. Gualdi, and A. Navarra, 2014: European blocking and Atlantic jet stream variability in the NCEP/NCAR reanalysis and the CMCC-CMS climate model. *Climate Dyn.,* **43,** 71–85. doi:10.1007/s00382-013-1873-y.

Dee, D. P., and Coauthors, 2011: The ERA-Interim reanalysis: configuration and performance of the data assimilation system. *Quart. J. Roy. Meteor. Soc.*, **137,** 553–597. doi:10.1002/qj.828.

Dufresne, J. L., and Coauthors, 2013: Climate change projections using the IPSL-CM5 Earth System Model: from CMIP3 to CMIP5. *Climate Dyn.,* **40,** 2123–2165. doi:10.1007/s00382-012-1636-1.

Dunkerton, T. J., 1997: The role of gravity waves in the quasi-biennial oscillation. *J. Geophys. Res.*, **102,** 26053–26076. doi:10.1029/96jd02999.

Dunkerton, T. J., 2001: Quasi-biennial and subbiennial variations of stratospheric trace constituents derived from HALOE observations. *J. Atmos. Sci.*, **58,** 7–25.

Accepted for publication in *Journal of Climate*. DOI10.1175/JCLI-D-19-0663.1.

Garfinkel, C. I., and D. L. Hartmann, 2007: Effects of the El Niño–Southern Oscillation and the Quasi-Biennial Oscillation on polar temperatures in the stratosphere. *J. Geophys. Res.*, **112,** D19112. doi:10.1029/2007jd008481.

Garfinkel, C. I., and D. L. Hartmann, 2011a: The Influence of the quasi-biennial oscillation on the troposphere in winter in a hierarchy of models. Part I: simplified dry GCMs. *J. Atmos. Sci.*, **68,** 1273–1289. doi:10.1175/2011jas3665.1.

Garfinkel, C. I., and D. L. Hartmann, 2011b: The Influence of the quasi-biennial oscillation on the troposphere in winter in a hierarchy of models. Part II: perpetual winter WACCM runs. *J. Atmos. Sci.*, **68,** 2026–2041. doi:10.1175/2011jas3702.1.

Garfinkel, C. I., T. A. Shaw, D. L. Hartmann, and D. W. Waugh, 2012: Does the Holton–Tan mechanism explain how the quasi-biennial oscillation modulates the Arctic polar vortex? *J. Atmos. Sci.*, **69,** 1713–1733. doi:10.1175/jas-d-11-0209.1.

Garfinkel, C. I., I. Weinberger, I. P. White, L. D. Oman, V. Aquila, and Y. K. Lim, 2018a: The salience of nonlinearities in the boreal winter response to ENSO: North Pacific and North America. *Climate Dyn.*, **52,** 4429–4446. doi:10.1007/s00382-018-4386-x.

Garfinkel, C. I., A. Gordon, L. D. Oman, F. Li, S. Davis, and S. Pawson, 2018b: Nonlinear response of tropical lower stratospheric temperature and water vapor to ENSO. *Atmos. Chem. Phys.*, **18,** 4597–4615, doi:10.5194/acp-18-4597-2018.

Garfinkel, C. I., C. Schwartz, D. I. Domeisen, S. W. Son, A. H. Butler, and I. P. White, 2018c: Extratropical atmospheric predictability from the quasi-biennial oscillation in subseasonal forecast models. J. Geophys. Res. Atmos., **123**, 7855–7866, doi: 10.1029/2018JD028724.

Geller, M. A., and Coauthors, 2016: Modeling the QBO—Improvements resulting from higher-model vertical resolution. *J. Adv. Model. Earth Syst.*, **8,** 1092–1105, doi:10.1002/2016MS000699.

Accepted for publication in *Journal of Climate*. DOI10.1175/JCLI-D-19-0663.1.

Giorgetta, M. A., E. Manzini, and E. Roeckner, 2002: Forcing of the quasi-biennial oscillation from a broad spectrum of atmospheric waves. *Geophys. Res. Lett.,* **29**, 1245. doi:10.1029/2002gl014756.

Giorgetta, M. A., E. Manzini, and E. Roeckner, M. Esch, and L. Begtsson, 2006: Climatology and forcing of the quasi-biennial oscillation in the MAECHAM5 model. *J. Climate,* **19**, 3882–3901. doi:10.1175/jcli3830.1.

Giorgetta, M. A., and Coauthors, 2013: Climate and carbon cycle changes from 1850 to 2100 in MPI-ESM simulations for the Coupled Model Intercomparison Project phase 5. *J. Adv. Model. Earth Syst.*, **5,** 572–597. doi:10.1002/Jame.20038.

Gong, D.-Y., S.-W. Wang, and J.-H., 2001: East Asian winter monsoon and Arctic Oscillation. *Geophys. Res. Lett.*, **28**, 2073–2076. doi: 10.1029/2000gl012311.

Gray, W. M., J. D. Sheaffer, and J. A. Knaff, 1992: Hypothesized mechanism for stratospheric QBO influence on ENSO variability. *Geophys. Res. Lett.*, **19,** 107–11. doi:10.1029/91gl02950.

Gray, L. J., T. J. Woollings, M. Andrews, and J. Knight, 2016: Eleven-year solar cycle signal in the NAO and Atlantic/European blocking. *Quart. J. Roy. Meteor. Soc.*, **142**, 1890–1903.

Gray, L. J., J. A. Anstey, Y. Kawatani, H. Lu, S. Osprey, and V. Schenzinger, 2018: Surface impacts of the quasi biennial oscillation. *Atmos. Chem. Phys.*, **18,** 8227–8247. doi:10.5194/acp-18-8227-2018.

Ho, C., H. Kim, J. Jeong, and S. Son, 2009: Influence of stratospheric quasi-biennial oscillation on tropical cyclone tracks in the western North Pacific. *Geophys. Res. Lett.*, **36**, L06702. doi:10.1029/2009gl037163.

Holt, L. A., M. J. Alexander, L. Coy, A. Molod, W. Putman, and S. Pawson, 2016: Tropical waves and the quasi-biennial oscillation in a 7-km global climate simulation. *J. Atmos. Sci.*, **73,** 3771–3783. doi:10.1175/jas-d-15-0350.1.

Accepted for publication in *Journal of Climate*. DOI10.1175/JCLI-D-19-0663.1.

Holton, J. R., and H. C. Tan, 1980: The Influence of the equatorial quasi-biennial oscillation on the global circulation at 50mb. *J. Atmos. Sci.*, **37,** 2200–2208.

Horinouchi, T., and S. Yoden, 1998: Wave-mean flow interaction associated with a QBO-like oscillation simulated in a simplified GCM. *J. Atmos. Sci.*, **55,** 502–526.

Hu, Z.-Z., B. Huang, J. L. Kinter, Z. Wu, and A. Kumar, 2011: Connection of the stratospheric QBO with global atmospheric geneal circulation and tropical SST. Part II: interdecadal variations. *Climate Dyn.*, **38,** 25–43, doi:10.1007/s00382-011-1073-6.

Huang, B., Z.-Z. Hu, J. L. Kinter, Z. Wu, and A. Kumar, 2011: Connection of stratospheric QBO with global atmospheric general circulation and tropical SST. Part I: methodology and composite life cycle. *Climate Dyn.*, **38,** 1–23. doi:10.1007/s00382-011-1250-7.

Huesmann, A. S., and M. H. Hitchman, 2001: The stratospheric quasi-biennial oscillation in the NCEP reanalyses: climatological structures. *J. Geophys. Res.*, **106**, 11859–11874.

Hurwitz, M. M., and Coauthors, 2014: Extra-tropical atmospheric response to ENSO in the CMIP5 models. *Climate Dyn.*, **43,** 3367–3376, doi:10.1007/s00382-014-2110-z.

Ineson, S., and A. A. Scaife, 2009: The role of the stratosphere in the European climate response to El Niño. *Nat. Geosci.*, **2**, 32–36. doi:10.1038/ngeo381.

Jones, D. B. A., H. R. Schneider, and M. B. McElroy, 1998: Effects of the quasi-biennial oscillation on the zonally averaged transport of tracers. *J. Geophys. Res.*, **103,** 11235–11249. doi:10.1029/98jd00682.

Kawatani, Y., and K. Hamilton, 2013: Weakened stratospheric quasibiennial oscillation driven by increased tropical mean upwelling. *Nature*, **497**, 478–481. doi:10.1038/nature12140.

Kawatani, Y., J. N. Lee, and K. Hamilton, 2014: Interannual variations of stratospheric water vapor in MLS observations and climate model simulations. *J. Atmos. Sci.*, **71**, 4072–4085. doi:10.1175/jas-d-14-0164.1.

Accepted for publication in *Journal of Climate*. DOI10.1175/JCLI-D-19-0663.1.

Kobayashi, S., and Coauthors, 2015: The JRA-55 reanalysis: General specifications and basic characteristics. *J. Meteor. Soc. Japan,* **93,** 5–48. doi:10.2151/jmsj.2015-001.

Kuhlbrodt, T., and Coauthors, 2018: The low-resolution version of HadGEM3 GC3.1: development and evaluation for global climate. *J. Adv. Model. Earth. Syst.*, **10,** 2865–2888. doi:10.1029/2018MS001370.

Labitzke, K., and M. Kunze, 2009: On the remarkable Arctic winter in 2008/2009. Geophys. Res. Lett., 114, D00I02. doi:10.1029/2009jd012273.

Li, F., Y. V. Vikhliaev, P. A. Newman, S. Pawson, J. Perlwitz, D. W. Waugh, and A. R. Douglass, 2016: Impacts of interactive stratospheric chemistry on Antarctic and Southern Ocean climate change in the Goddard Earth Observing System, version 5 (GEOS-5). *J. Climate*, **29,** 3199–3218. doi:10.1175/jcli-d-15-0572.1.

Liess, S., and M. A. Geller, 2012: On the relationship between QBO and distribution of tropical deep convection. *J. Geophys. Res.*, **117,** D03108. doi:10.1029/2011jd016317.

Lindzen, R. S., and J. R. Holton, 1968: A theory of the quasi-biennial oscillation. *J. Atmos. Sci.*, **25**, 1095–1107.

Liu, H.-L., and Coauthors, 2018: Development and validation of the Whole Atmosphere Community Climate Model with thermosphere and ionosphere extension (WACCM-X 2.0). *J. Adv. Model. Earth Syst.*, **10**, 381–402. doi:10.1002/2017ms001232.

Luo, M., J. M. Russell, and T. Y. W. Huang, 1997: Halogen occultation experiment observations of the quasi-biennial oscillation and the effects of Pinatubo aerosols in the tropical stratosphere. *J. Geophys. Res.*, **102,** 19187–19198. doi:10.1029/97jd01015.

Marsh, D. R., M. J. Mills, D. E. Kinnison, J. F. Lamarque, N. Calvo, and L. M. Polvani, 2013: Climate change from 1850 to 2005 simulated in CESM1(WACCM). *J. Climate*, **26,** 7372–7391. doi:10.1175/JCLI-D-12-00558.1.

Accepted for publication in *Journal of Climate*. DOI10.1175/JCLI-D-19-0663.1.

Marshall, A. G., and A. A. Scaife, 2009: Impact of the QBO on surface winter climate. *J. Geophys. Res.*, **114**, D18110. doi:10.1029/2009JD011737.

Martin, G. M., and Coauthors, 2011: The HadGEM2 family of Met Office Unified Model climate configurations. *Geosci. Model Dev.*, **4,** 723–757. doi:10.5194/gmd-4-723-2011.

Maruyama, T., 1994: Upward transport of westerly momentum due to disturbances of the equatorial lower stratosphere in the period range of about 2 days—Singapore data analysis for 1983–1993, *J. Meteor. Soc. Japan.*, **72**, 423–432.

Massonnet, F., M. Ménégoz, M. Acosta, X. Yepes-Arbós, E. Exarchou, and F. J. Doblas-Reyes, 2019: Replicability of the EC-Earth3 Earth System Model under a change in computing environment. *Geosci. Model Dev. Discuss.***,** 1–19. doi:10.5194/gmd-2019-91.

Matthes, K., D. R. Marsh, R. R. Garcia, D. E. Kinnison, F. Sassi, and S. Walters, 2010: Role of the QBO in modulating the influence of the 11 year solar cycle on the atmosphere using constant forcings. *J. Geophys. Res.*, **115,** D18110. doi:10.1029/2009jd013020.

Naito, Y., 2002: Planetary wave diagnostics on the QBO effects on the deceleration of the polar-night jet in the southern hemisphere. *J. Meteor. Soc. Japan*, **80**, 985–995. doi:10.2151/jmsj.80.985.

Naujokat, B., 1986: An update of the observed quasi-biennial oscillation of the stratospheric winds over the tropics. *J. Atmos. Sci.*, **43,** 1873–1877.

Naoe, H., and K. Yoshida, 2019: Influence of quasi-biennial oscillation on the boreal winter extratropical stratosphere in QBOi experiments. *Quart. J. Roy. Meteor. Soc.*, in press. doi:10.1002/qj.3591.

Newman, P. A., L. Coy, S. Pawson, and L. R. Lait, 2016: The anomalous change in the QBO in 2015–2016. *Geophys. Res. Lett.*, **43,** 8791–8797. doi:10.1002/2016gl070373.

Osprey, S. M., and Coauthors, 2016: An unexpected disruption of the atmospheric quasi-biennial oscillation. *Science*, **353,** 1424–1427. doi:10.1126/science.aah4156.

Accepted for publication in *Journal of Climate*. DOI10.1175/JCLI-D-19-0663.1.

O'Sullivan, D., and T. J. Dunkerton, 1997: The influence of the quasi-biennial oscillation on global constituent distributions. *J. Geophys. Res.*, **102,** 21731–21743. doi:10.1029/97jd01689.

Politowicz, P. A., and M. H. Hitchman, 1997: Exploring the effects of forcing quasi-biennial oscillations in a two-dimensional model. *J. Geophys. Res.*, **102,** 16481–16497. doi:10.1029/97jd00693.

Rajendran, K., I. M. Moroz, P. L. Read, and S. M. Osprey, 2016: Synchronisation of the equatorial QBO by the annual cycle in tropical upwelling in a warming climate. *Quart. J. Roy. Meteor. Soc.*, **142,** 1111–1120. doi:10.1002/qj.2714.

Rajendran, K., I. M. Moroz, S. M. Osprey, and P. L. Read, 2018: Descent rate models of the synchronization of the quasi-biennial oscillation by the annual cycle in tropical upwelling. *J. Atmos. Sci.*, **75,** 2281–2297. doi:10.1175/jas-d-17-0267.1.

Randel, W. J., and F. Wu, 1996: Isolation of the ozone QBO in SAGE II data by singular-value decomposition. *J. Atmos. Sci.*, **53,** 2546–2559.

Randel, W. J., F. Wu, J. M. Russell, A. Roche, and J. W. Waters, 1998: Seasonal cycles and QBO variations in stratospheric CH_4 and H_2O observed in UARS HALOE data. *J. Atmos. Sci.*, **55,** 163–185.

Randel, W. J., F. Wu, R. Swinbank, J. Nash, and A. O'Neill, 1999: Global QBO circulation derived from UKMO stratospheric analyses. *J. Atmos. Sci.*, **56,** 457–474.

Rao, J., and R.-C. Ren, 2016: A decomposition of ENSO's impacts on the northern winter stratosphere: Competing effect of SST forcing in the tropical Indian Ocean. *Climate Dyn.*, **46**, 3689–3707.

Rao, J., and R.-C. Ren, 2017: Parallel comparison of the 1982/83, 1997/98, and 2015/16 super El Niños and their effects on the extratropical stratosphere. *Adv Atmos. Sci.*, **34**, 1121–1133. doi:10.1007/s00376-017-6260-x.

Accepted for publication in *Journal of Climate*. DOI10.1175/JCLI-D-19-0663.1.

Rao, J., and R.-C. Ren, 2018: Varying stratospheric responses to tropical Atlantic SST forcing from early to late winter. *Climate Dyn*., **51**, 2079–2096. doi: 10.1007/s00382-017-3998-x.

Rao, J., Y. Yu, D. Guo, C. Shi, D. Chen, and D. Hu, 2019a: Evaluating the Brewer–Dobson circulation and its responses to ENSO, QBO, and the solar cycle in different reanalyses. *Earth Planet. Phys*., **3**, 166–181. doi: 10.26464/epp2019012.

Rao, J., C. I. Garfinkel, and R. Ren, 2019b: Modulation of the northern winter stratospheric El Niño–Southern Oscillation teleconnection by the PDO. *J. Climate*, **32**, 5761–5783. doi: 10.1175/jcli-d-19-0087.1.

Richter, J. H., A. Solomon, and J. T. Bacmeister, 2014a: On the simulation of the quasi-biennial oscillation in the Community Atmosphere Model, version 5. *J. Geophys. Res. Atmos.*, **119,** 3045–3062, doi:10.1002/2013jd021122.

Richter, J. H., A. Solomon, and J. T. Bacmeister, 2014b: Effects of vertical resolution and nonorographic gravity wave drag on the simulated climate in the Community Atmosphere Model, version 5. *J. of Adv. Model. Earth Syst.*, **6,** 357–383. doi: 10.1002/2013ms000303.

Rind, D., J. Jonas, N. K. Balachandran, G. A. Schmidt, and J. Lean, 2014: The QBO in two GISS global climate models: 1. generation of the QBO. *J. Geophys. Res. Atmos.*, **119,** 8798–8824. doi:10.1002/2014jd021678.

Ruzmaikin, A., J. Feynman, X. Jiang, Y. L. Yung, 2005: Extratropical signature of the quasi-biennial oscillation. *J. Geophys. Res.*, **110**, D11111. doi: 10.1029/2004jd005382.

Salby, M., and P. Callaghan, 2000: Connection between the solar cycle and the QBO: the missing link. *J. Climate*, **13,** 2652–2662.

Scaife, A. A., N. Butchart, C. D. Warner, D. Stainforth, W. Norton, and J. Austin, 2000: Realistic quasi-biennial oscillations in a simulation of the global climate. *Geophys. Res. Lett.*, **27,** 3481–3484. doi:10.1029/2000gl011625.

Accepted for publication in *Journal of Climate*. DOI10.1175/JCLI-D-19-0663.1.

Scaife, A. A., S. Ineson, J. R. Knight, L. Gray, K. Kodera, and D. M. Smith, 2013: A mechanism for lagged North Atlantic climate response to solar variability. *Geophys. Res. Lett.*, **40,** 434–439, doi:10.1002/grl.50099.

Schenzinger, V., S. Osprey, L. Gray, and N. Butchart, 2017: Defining metrics of the quasi-biennial oscillation in global climate models. *Geosci. Model Dev.*, **10,** 2157–2168. doi:10.5194/gmd-10-2157-2017.

Schirber, S., E. Manzini, T. Krismer, and M. Giorgetta, 2014: The quasi-biennial oscillation in a warmer climate: sensitivity to different gravity wave parameterizations. *Climate Dyn*., **45**, 825–836, doi:10.1007/s00382-014-2314-2.

Séférian, R., and Coauthors, 2016: Development and evaluation of CNRM Earth system model – CNRM-ESM1. *Geosci. Model Dev.*, **9,** 1423–1453. doi:10.5194/gmd-9-1423-2016.

Silverman, V., N. Harnik, K. Matthes, S. W. Lubis, and S. Wahl, 2018: Radiative effects of ozone waves on the Northern Hemisphere polar vortex and its modulation by the QBO. Atmos. Chem. Phys., **18**, 6637–6659, doi: 10.5194/acp-18-6637-2018.

Solomon, A., J. H. Richter, and J. T. Bacmeister, 2014: An objective analysis of the QBO in ERA-Interim and the Community Atmosphere Model, version 5. *Geophys. Res. Lett.*, **41,** 7791–7798. doi: 10.1002/2014gl061801.

Son, S., Y. Lim, C. Yoo, H. H. Hendon, and J. Kim, 2017: Stratospheric control of the Madden-Julian Oscillation. *J. Climate*, **30**, 1909–1922. doi: 10.1175/jcli-d-16-0620.1.

Takahashi, M., and B. A. Boville, 1992: A 3-dimensional simulation of the equatorial quasi-biennial oscillation. *J. Atmos. Sci.*, **49,** 1020–1035.

Takahashi, M., 1996: Simulation of the stratospheric quasi-biennial oscillation using a general circulation model. *Geophys. Res. Lett.*, **23,** 661–664. doi:10.1029/95gl03413.

Takahashi, M., 1999: Simulation of the quasi-biennial oscillation in a general circulation model. *Geophys. Res. Lett.*, **26,** 1307–1310, doi:10.1029/1999gl900188.

Accepted for publication in *Journal of Climate*. DOI10.1175/JCLI-D-19-0663.1.

Tatebe, H., and Coauthors, 2019: Description and basic evaluation of simulated mean state, internal variability, and climate sensitivity in MIROC6. *Geosci. Model Dev.*, **12,** 2727–2765. doi:10.5194/gmd-12-2727-2019.

Thompson, D. W. J., and J. M. Wallace, 2000: Annular modes in the extratropical circulation. Part I: Month-to-month variability. *J. Climate*, **13,** 1000–1016.

Untch, A., and Coauthors, 1998: Increased stratospheric resolution in the ECMWF forecasting system. *ECMWF Newsletter*, **82**, 2–8.

Voldoire, A., and Coauthors, 2019: Evaluation of CMIP6 DECK experiments with CNRM-CM6-1. *J. Adv. in Model. Earth Syst.*, **11**, in press. doi:10.1029/2019ms001683.

Wallace, J. M., and V. E. Kousky, 1968: Observational evidence of Kelvin waves in the tropical stratosphere. *J. Atmos. Sci.*, **25,** 900–907.

Wallace, J. M., R. L. Panetta, and J. Estberg, 1993: Representation of the equatorial stratospheric quasi-Biennial oscillation in EOF phase space. *J. Atmos. Sci.*, **50,** 1751–1762.

Watanabe, S., and Coauthors, 2011: MIROC-ESM 2010: model description and basic results of CMIP5-20c3m experiments. *Geosci. Model Dev.*, **4,** 845–872. doi: 10.5194/Gmd-4-845-2011.

Watanabe, S., K. Hamilton, S. Osprey, Y. Kawatani, and E. Nishimoto, 2018: First successful hindcasts of the 2016 disruption of the stratospheric quasi-biennial oscillation. *Geophys. Res. Lett.*, **45,** 1602–1610. doi:10.1002/2017gl076406.

Watson, P. A. G., and L. J. Gray, 2014: How does the quasi-biennial oscillation affect the stratospheric polar vortex? *J. Atmos. Sci.*, **71,** 391–409. doi:10.1175/jas-d-13-096.1.

Wei, K., W. Chen, and R. Huang, 2007: Association of tropical Pacific sea surface temperatures with the stratospheric Holton-Tan oscillation in the Northern Hemisphere winter. *Geophys. Res. Lett.*, **34**, L16814. doi:10.1029/2007gl030478.

Accepted for publication in *Journal of Climate*. DOI10.1175/JCLI-D-19-0663.1.

Weinberger, I., C. I. Garfinkel, I. P. White, and L. D. Oman, 2019: The salience of nonlinearities in the boreal winter response to ENSO: Arctic stratosphere and Europe. *Climate Dyn.*, in press. doi:10.1007/s00382-019-04805-1.

White, I. P., H. Lu, N. J. Mitchell, and T. Phillips, 2015: Dynamical response to the QBO in the northern winter stratosphere: signatures in wave forcing and eddy fluxes of potential vorticity. *J. Atmos. Sci.*, **72**, 4487–4507. doi:10.1175/jas-d-14-0358.1.

White, I. P., H. Lu H, N. J. Mitchell, 2016: Seasonal evolution of the QBO induced wave forcing and circulation anomalies in the northern winter stratosphere. *J. Geophys. Res. Atmos.*, **121**, 10411–10431. doi:10.1002/2015jd024507.

Wu, T., and Coauthors, 2019: The Beijing Climate Center Climate System Model (BCC-CSM): the main progress from CMIP5 to CMIP6. *Geosci. Model Dev.*, **12,** 1573–1600. doi:10.5194/gmd-12-1573-2019.

Yoo, C., and S.-W. Son, 2016: Modulation of the boreal wintertime Madden-Julian oscillation by the stratospheric quasi-biennial oscillation. *Geophys. Res. Lett.*, **43**, 1392–1398. doi: https://doi.org/10.1002/2016gl067762.

Yukimoto, S., and Coauthors, 2019: The Meteorological Research Institute earth system model version 2.0, MRI-ESM2.0: description and basic evaluation of the physical component. *J. Meteor. Soc. Japan*, **97,** 931–965, doi:10.2151/jmsj.2019-051.

Accepted for publication in *Journal of Climate*. DOI 10.1175/JCLI-D-19-0663.1.

Table 1. Selected QBO-resolving CMIP5/6 models used in this study. The integration time span for CMIP5/6 is 1850–2005/1850–2014 in the historical run except that only a 230-yr coupled run with the greenhouse gas and ozone-depleting substance forcings fixed at 1950 levels is available for the GEOSCCM model.

Model	**Affiliation and nationality**	**Horizontal resolution (latitude × longitude)**	**Top (total levels and levels between 100–1hPa)**	**Reference**
CESM1-WACCM	NSF-DOE-NCAR, USA	F19 (96×144)	5.1×10^{-6} hPa (L66, 23)	Marsh et al. 2013
CMCC-CMS	CMCC, Italy	T63 (96×192)	0.01 hPa (L95, 44)	Davini et al. 2014
GEOSCCM	NASA, USA	2×2.5° (90×144)	0.01 hPa (L72, 23)	Li et al. 2016
HadGEM2-CCS	MOHC, UK	N96 (144×192)	85 km (L60, 23)	Martin et al. 2011
MIROC-ESM-CHEM	CCSR/NIES-AORI /UT-JAMSTEC, Japan	T42 (64×128)	0.0036 hPa (L80, 44)	Watanabe et al. 2011
MIROC-ESM	Above	Above	Above	Above
MPI-ESM-MR	MPI, Germany	T63 (96×192)	0.01 hPa (L95, 44)	Giorgetta et al. 2013
BCC-CSM2-MR	CMA-BCC, China	T106 (160×320)	1.46 hPa (L46, 23)	Wu et al. 2019
CESM2-WACCM	NSF-DOE-NCAR, USA	F09 (192×288)	4.5×10^{-6} hPa (L70, 23)	Liu et al. 2018
CNRM-CM6-1	CNRM, France	T_L127 (128×256)	0.01 hPa (L91, 29)	Voldoire et al. 2019
CNRM-ESM2-1	Above	Above	Above	Séférian et al. 2016
EC-Earth3	EC-Earth Consortium, Europe	T_L255 (256×512)	0.01hPa (L91, 29)	Massonnet et al. 2019
IPSL-CM6A-LR	IPSL, France	N96 (143×144)	80 km (L79, 25)	Dufresne et al. 2013
MIROC6	CCSR/NIES-AORI /UT-JAMSTEC, Japan	T85 (128×258)	0.004hPa (L81, 37)	Tatebe et al. 2019
MRI-ESM2-0	JMA-MRI, Japan	T_L159 (160×320)	0.01hPa (L80, 29)	Yukimoto et al. 2019
UKESM1-0-LL	MOHC/NCAS, UK	N96 (144×192)	85 km (L85, 29)	Kuhlbrodt et al. 2018

Accepted for publication in *Journal of Climate*. DOI10.1175/JCLI-D-19-0663.1.

Table 2. Westerly QBO (QBO30 ≥ 5 m s^{-1}) and easterly QBO (QBO30 ≤ -5 m s^{-1}) winter sizes and their ratio in the reanalyses and CMIP5/6 models. The timespan is 1979–2014 (1958–2014) for ERA-Interim (JRA55). Refer to Table 1 for the timespan for models. The last column shows the composite difference in the winter-mean Niño3.4 (5°S–5°N, 170–120°W) index between EQBO and WQBO.

Model	**EQBO**	**WQBO**	**Ratio**	**Composite Niño3.4**
ERA-Interim	14	14	1.00	-0.04
JRA55	24	20	1.20	0.02
CESM1-WACCM	70	72	0.97	-0.01
CMCC-CMS	48	40	1.20	0.40
GEOSCCM	99	105	0.94	-0.002
HadGEM2-CCS	56	72	0.78	-0.06
MIROC-ESM-CHEM	58	65	0.89	-0.02
MIROC-ESM	66	60	1.10	-0.01
MPI-ESM-MR	66	68	0.97	0.05
BCC-CSM2-MR	40	50	0.80	-0.03
CESM2-WACCM	47	55	0.94	-0.43
CNRM-CM6-1	59	57	1.04	-0.01
CNRM-ESM2-1	56	57	0.98	0.10
EC-Earth3	59	68	0.87	0.05
IPSL-CM6A-LR	63	72	0.88	-0.15
MIROC6	59	70	0.84	-0.11
MRI-ESM2-0	70	74	0.95	0.10
UKESM1-0-LL	71	81	0.91	0.15

Accepted for publication in *Journal of Climate*. DOI 10.1175/JCLI-D-19-0663.1.

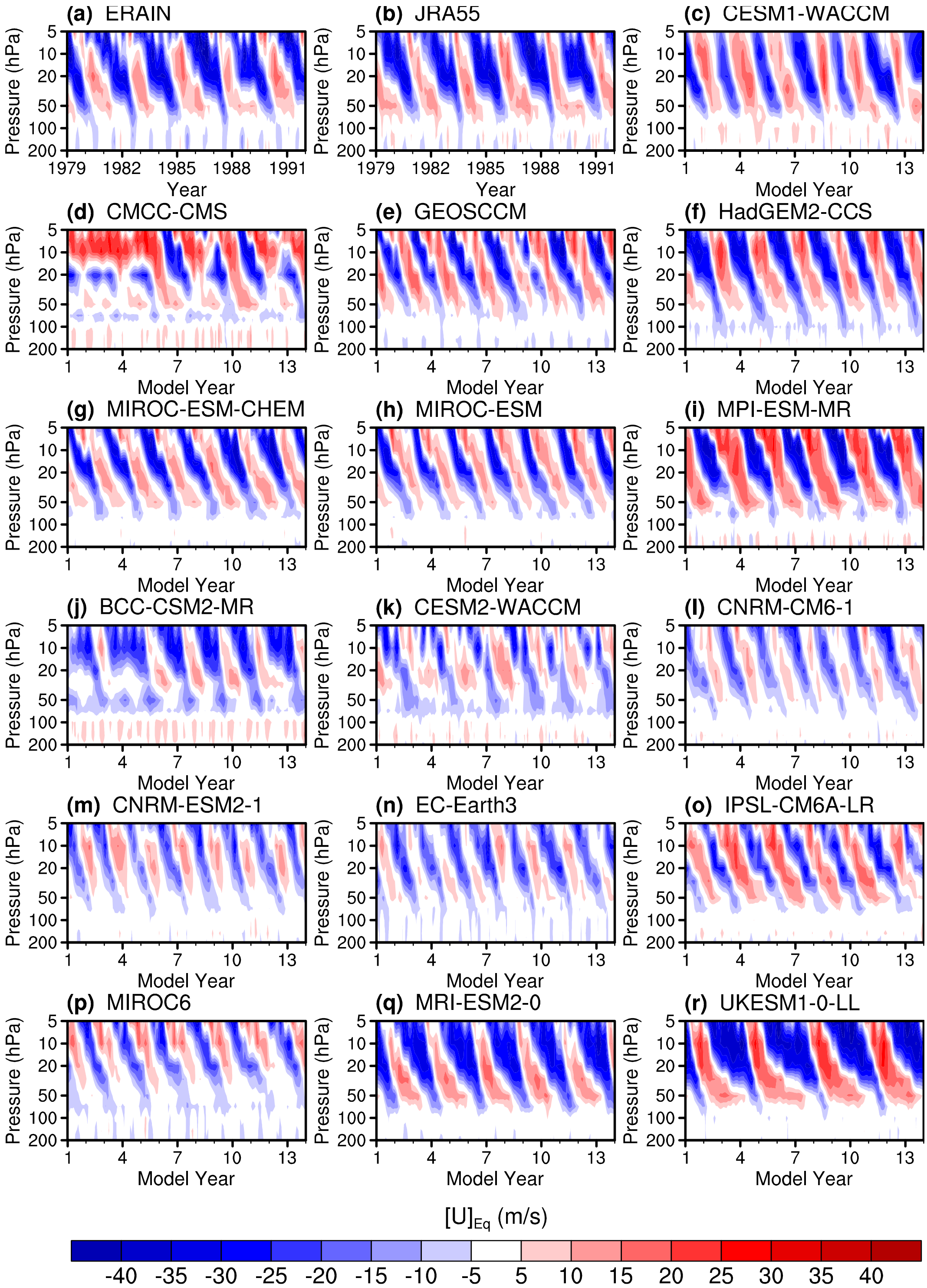

Fig. 1. Pressure-time evolution of the equatorial (5°S–5°N) zonal-mean zonal winds from 200–5hPa in the selected 13 years for (a, b) two reanalyses, (c–i) seven CMIP5 models, and (j–r) nine CMIP6 models. Considering that the historical runs from CMIP5/6 models are very long, only the first 13-yr data are shown for models. ERA-Intermin and JRA55 reanalyses are shown as a reference for QBO-resolving CMIP5/6 models.

Accepted for publication in *Journal of Climate*. DOI10.1175/JCLI-D-19-0663.1.

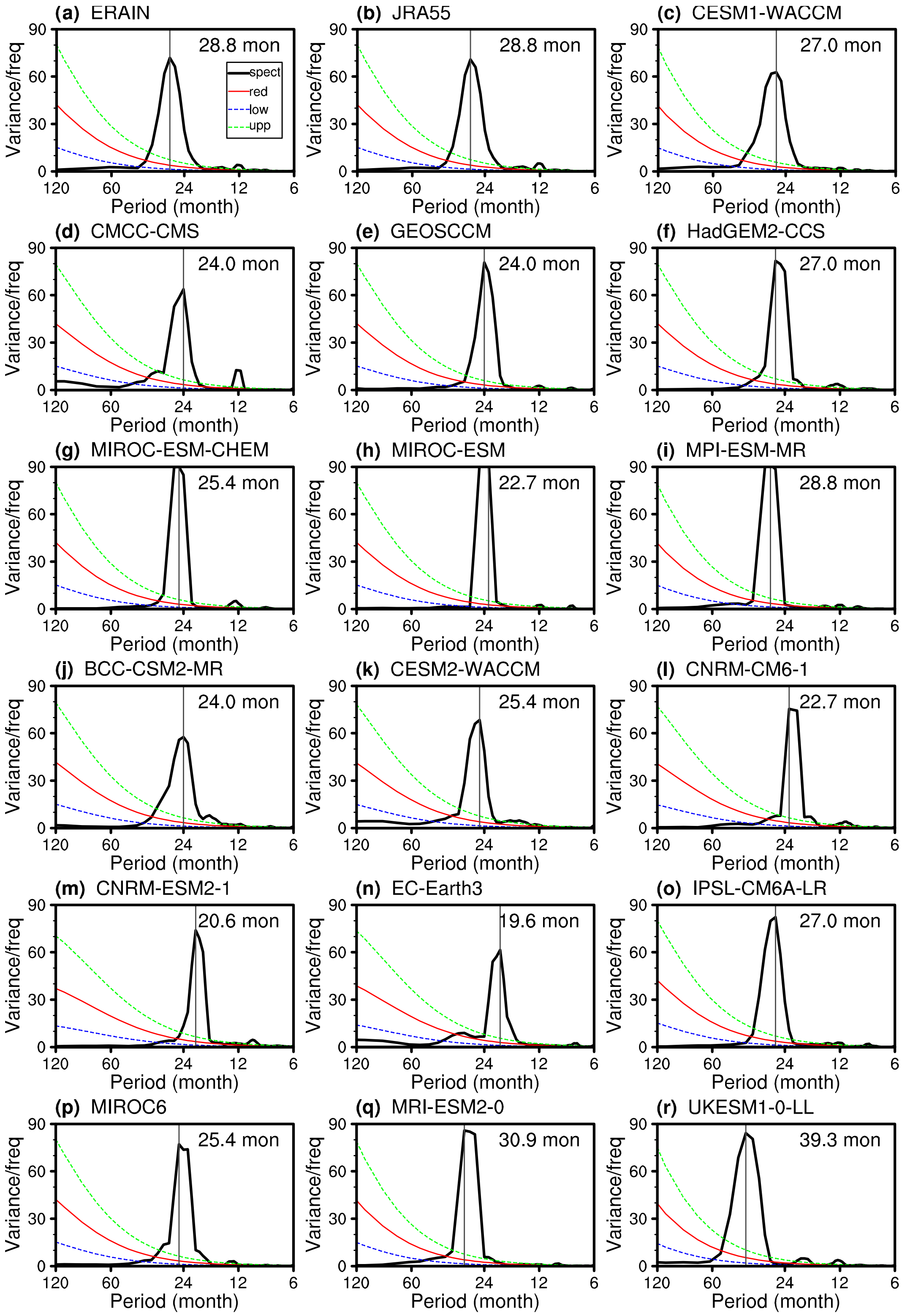

Fig. 2. Spectral analysis on the QBO index defined as the zonal-mean zonal wind anomalies over the equator at 30 hPa (QBO30) for (a, b) two reanalyses, (c–i) seven CMIP5 models, and (j–r) nine CMIP6 models. The dominant period is marked with a vertical line and printed on the top right for each dataset. The black thick curve is the power spectra of the QBO30, the red solid curve is red noise, and the blue and green dashed curves are the lower (5%) and upper (95%) confidence bounds.

Accepted for publication in *Journal of Climate*. DOI10.1175/JCLI-D-19-0663.1.

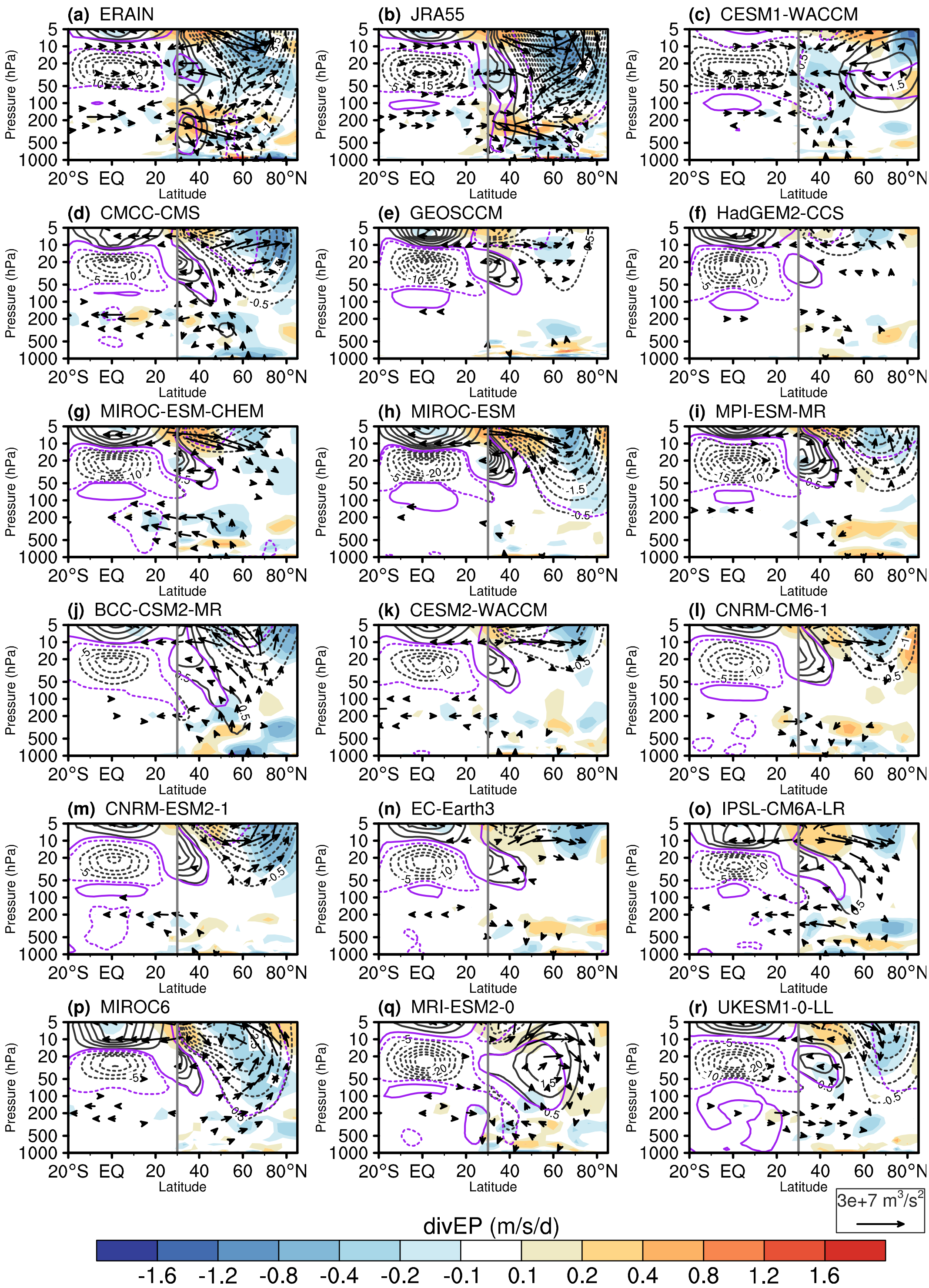

Fig. 3. Composite differences in the zonal-mean zonal wind anomalies (contours; units: m s^{-1}), in the scaled E-P flux anomalies (F_y/ρ_0, $100 \times F_z/\rho_0$; vectors; units: m^3 s^{-2}), and in the E-P flux divergence anomalies (shadings; units: m s^{-1} d^{-1}) during early winter (Nov–Jan) between the easterly QBO30 and westerly QBO30 phase. The purple lines mark the wind differences at the 95% confidence level according to the two-sided Student's *t*-test. Considering the QBO winds decrease exponentially with latitude, the contour interval is 5 m s^{-1} in the tropics (left to the vertical gray line) but 0.5 m s^{-1} in mid-to-high latitudes (right to the vertical gray line). The zero contours are skipped for clarity.

Accepted for publication in *Journal of Climate*. DOI 10.1175/JCLI-D-19-0663.1.

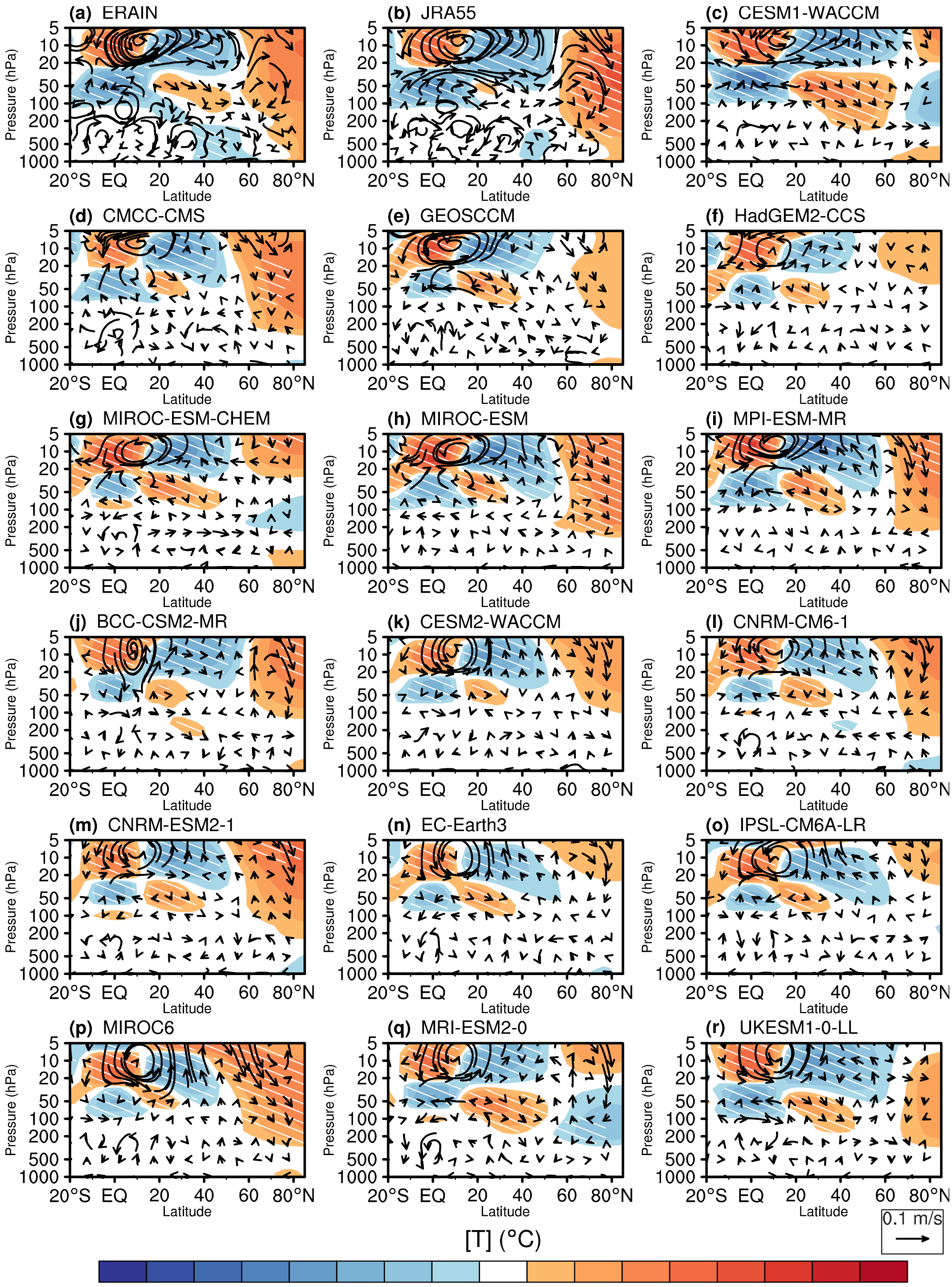

Fig. 4. Composite differences in the zonal-mean temperature anomalies (shadings; units: °C) and in the scaled residual velocity anomalies ($\bar{v}^*$, $200 \times \bar{w}^*$; curved arrows; units: m s^{-1}) during early winter (Nov–Jan) between the easterly QBO30 and westerly QBO30 phase. The hatched regions mark the temperature anomalies at the 95% confidence level according to the two-sided Student's *t*-test.

Accepted for publication in *Journal of Climate*. DOI10.1175/JCLI-D-19-0663.1.

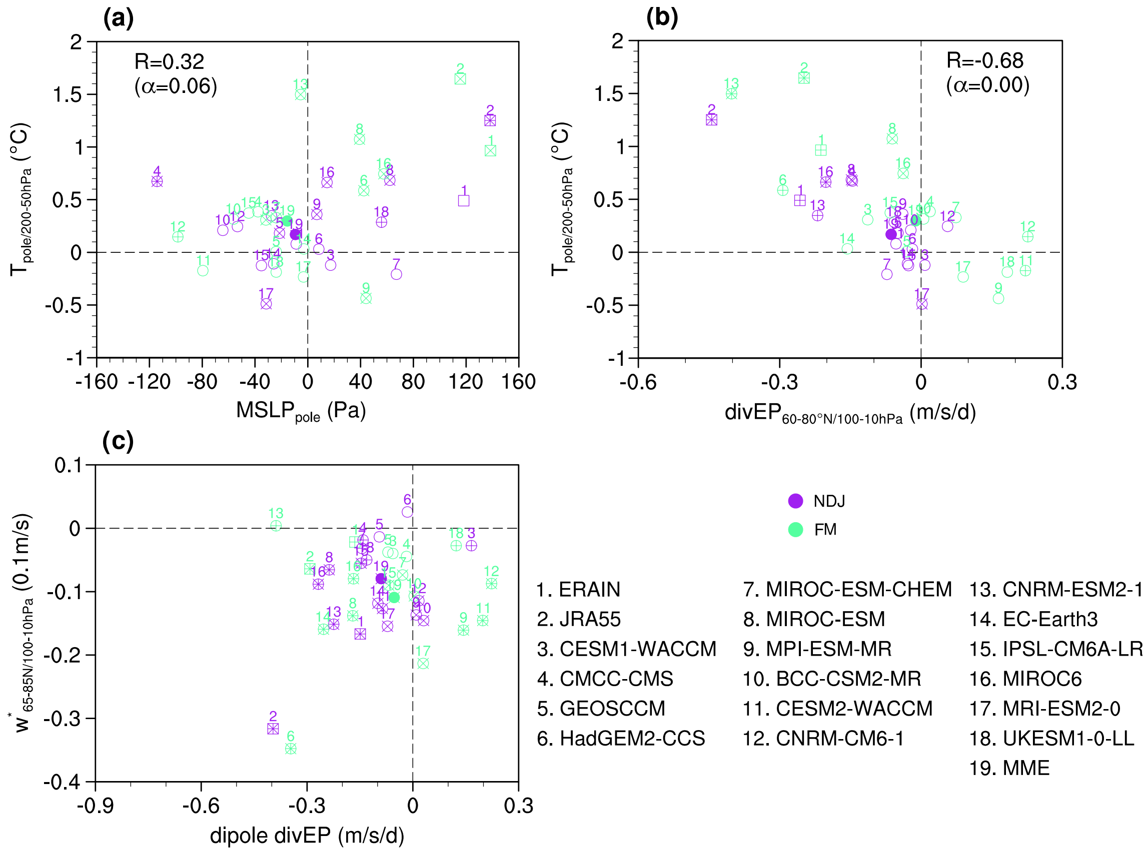

Fig. 5. Evaluation of the composite differences between easterly and westerly QBO30 during early winter (Nov–Jan, NDJ, in purple) and late winter (Feb–Mar, FM, in green) for different pairs of variables. (a) scatterplot of the polar mean sea level pressure (MSLP) vs. the lower stratospheric temperature over the Arctic (60–90°N, 200–50hPa). (b) scatterplot of the E-P flux divergence in the circumpolar stratosphere (60–80°N, 100–10hPa) vs. the polar lower stratospheric temperature (60–90°N, 200–50hPa). (c) scatterplot of the stratospheric E-P flux divergence dipole (difference between 60–80°N, 100–10hPa and 30–50°N, 30–10hPa) vs. the polar residual vertical velocity (65–85°N, 100–10hPa). The multi-model ensemble (MME) is shown in filled circles and the reanalysis open squares for clarity. The plus (cross) sign denotes the composite value of the *x*- (*y*-)axis at the 95% confidence level. The font/marker color denotes the subseason studied (purple: NDJ; green: FM), and the number above the scattered point marks the data source. The multi-model correlation between each pair of variables (R) and its significance level (α) are also printed if the correlation reaches a ≥90% confidence level.

Accepted for publication in *Journal of Climate*. DOI10.1175/JCLI-D-19-0663.1.

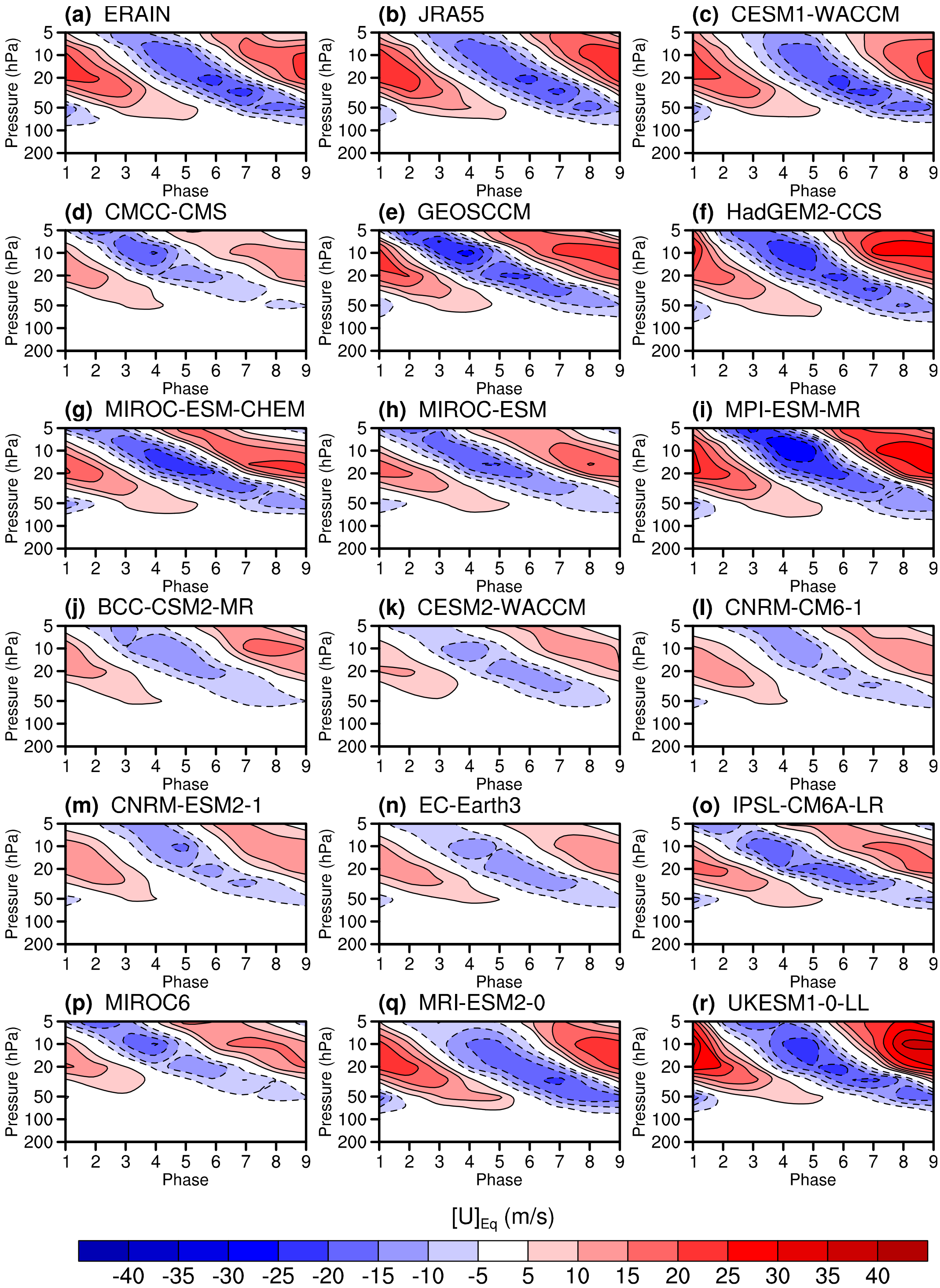

Fig. 6. Composite pressure–phase evolutions of the equatorial zonal wind anomalies (units: m s^{-1}) from 200–5hPa, phase 1–phase 8 (phase 9 is identical to phase 1) for (a, b) the two reanalyses and (c–r) 16 CMIP5/6 models. The eight phases of QBO are based on the QBO30 index and its tendency.

Accepted for publication in *Journal of Climate*. DOI10.1175/JCLI-D-19-0663.1.

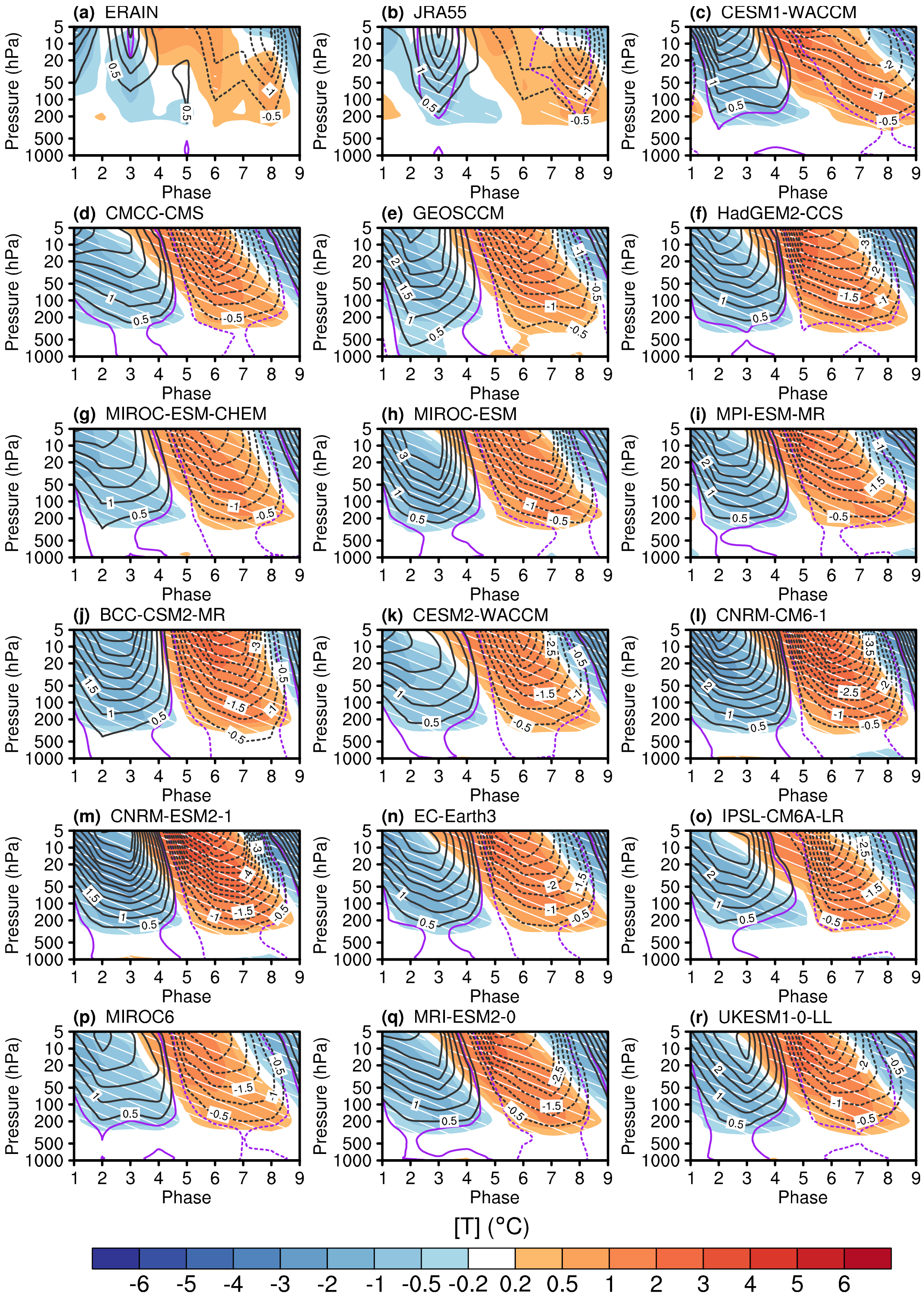

Fig. 7. Composite pressure–phase evolutions of polar cap temperature anomalies (60–90°N; shadings; units: °C) and circumpolar zonal wind anomalies (55–75°N; contours; units: m s^{-1}; interval: 0.5; zero skipped) during the extended winter (November–March) for (a) the two reanalyses and (c–r) 16 CMIP5/6 models. The hatched regions mark the temperature anomalies at the 95% confidence level according to the two-sided Student's *t*-test.

Accepted for publication in *Journal of Climate*. DOI10.1175/JCLI-D-19-0663.1.

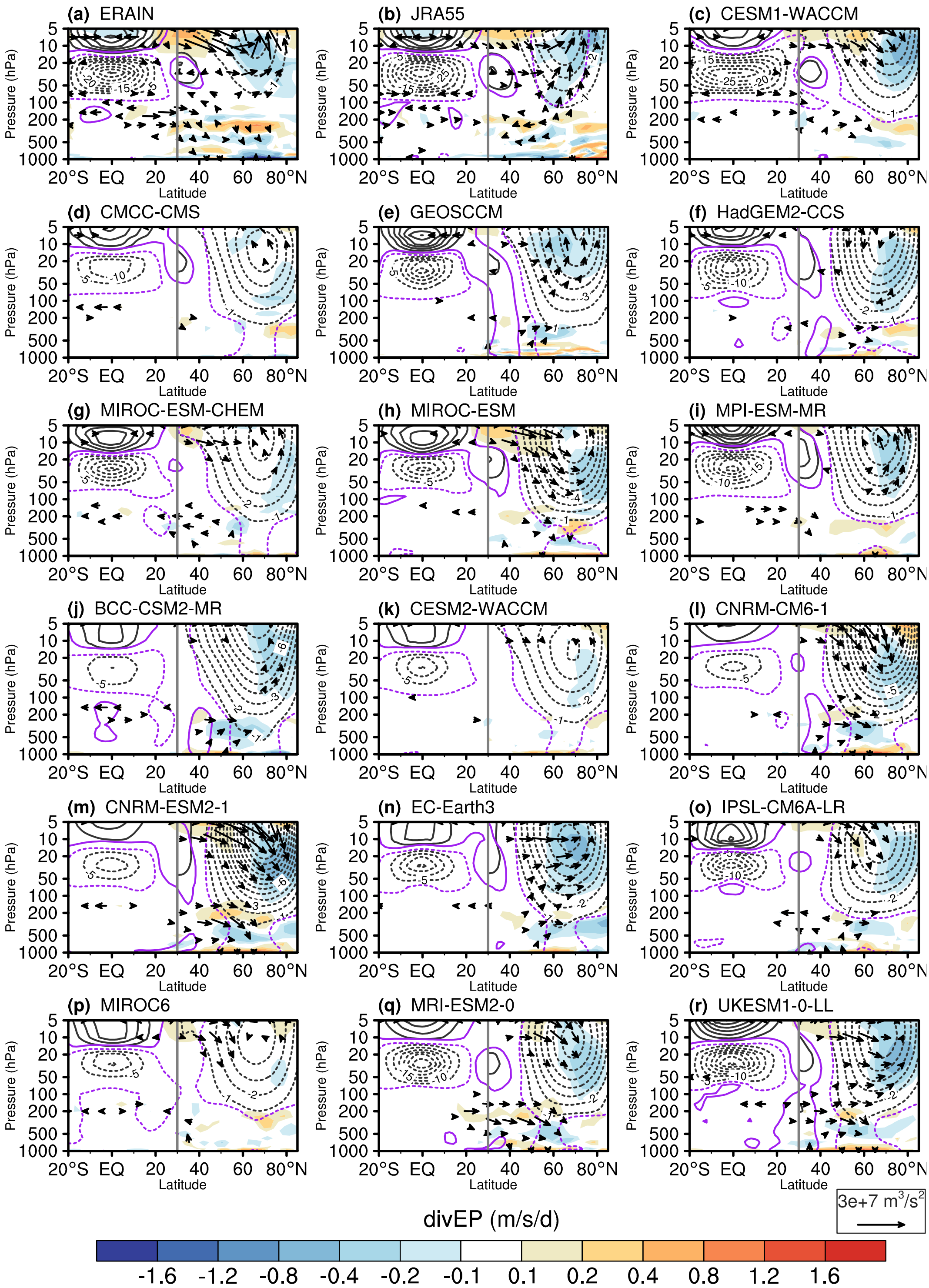

Fig. 8. As in Fig. 3 but for composite differences between QBO phase 7 and phase 3 during the extended winter (November–March). Note that the contour interval in mid-to-high latitudes (right to the vertical gray line, 1 m s^{-1}) is different from Fig. 3. The zero contours are skipped for clarity.

Accepted for publication in *Journal of Climate*. DOI10.1175/JCLI-D-19-0663.1.

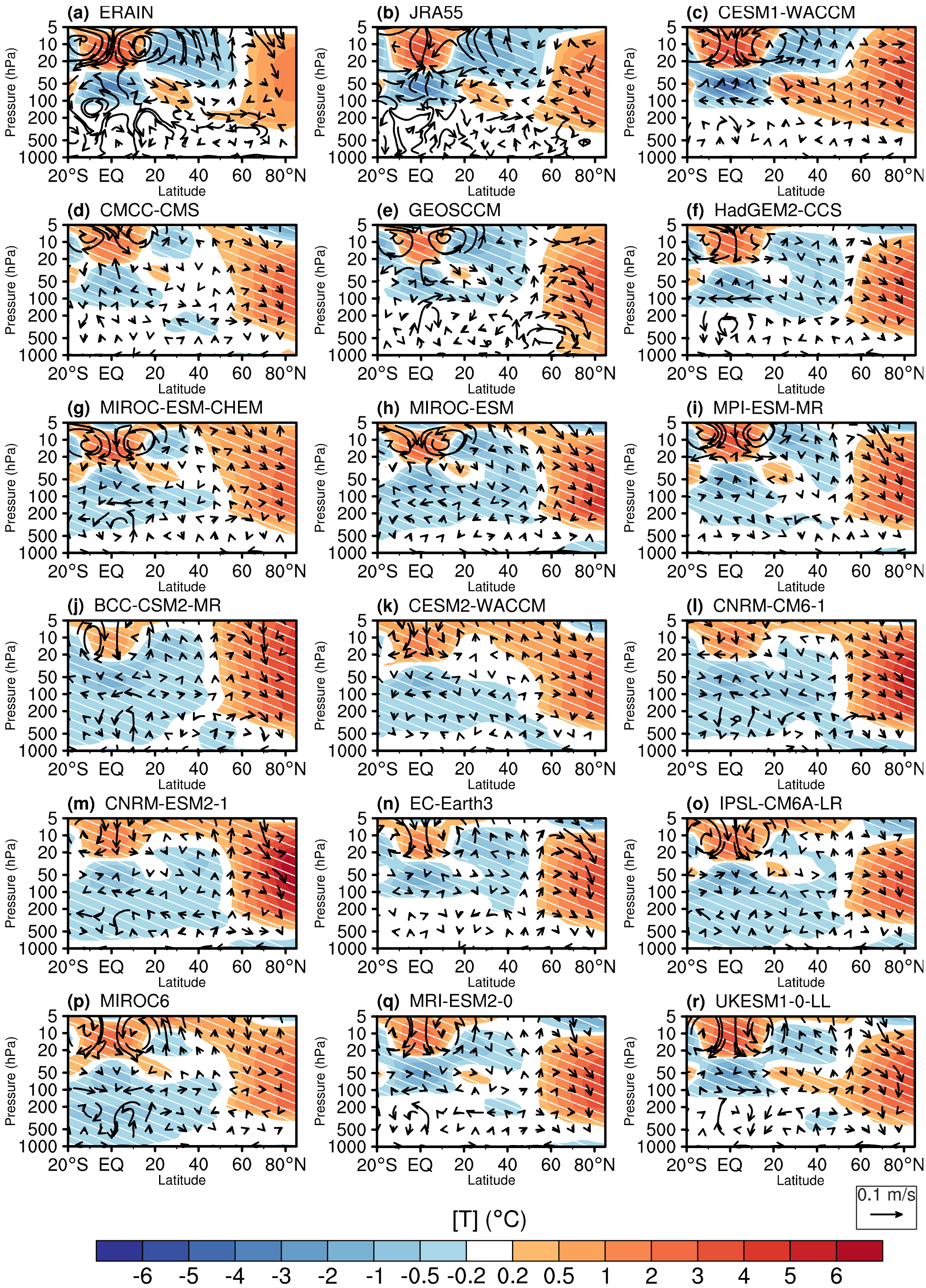

Fig. 9. As in Fig. 4 but for composite differences between QBO phase 7 and phase 3 during the extended winter (November–March).

Accepted for publication in *Journal of Climate*. DOI 10.1175/JCLI-D-19-0663.1.

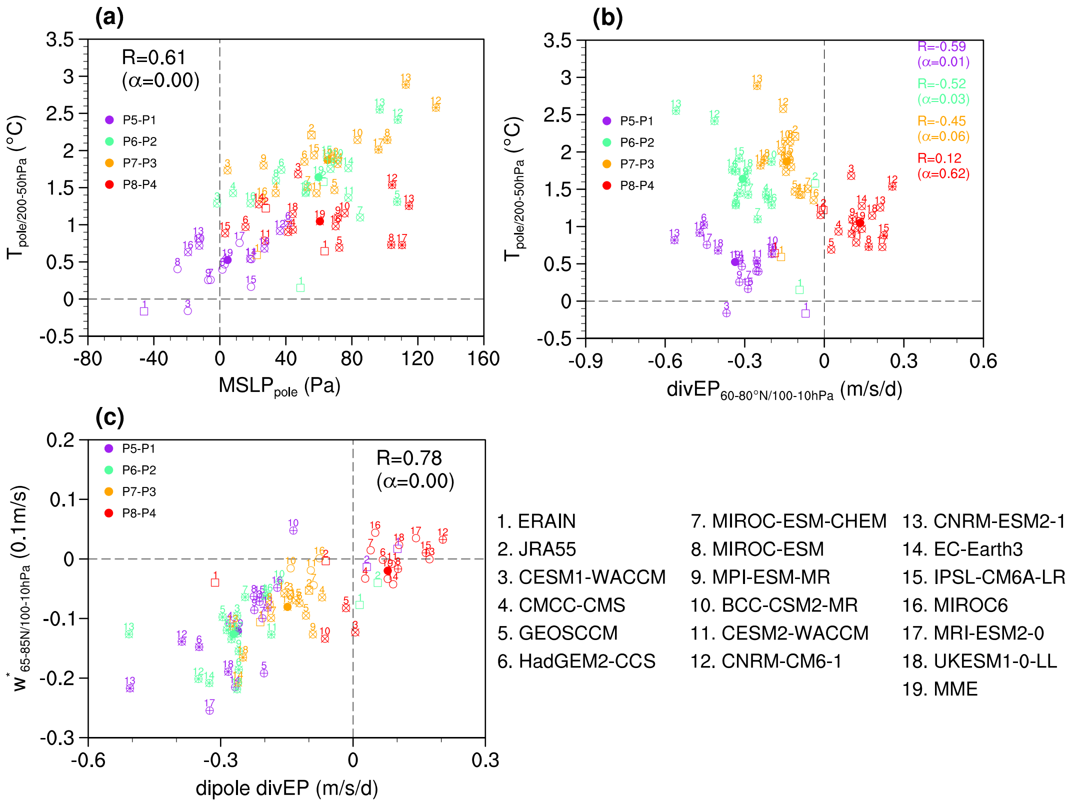

Fig. 10. As in Fig. 5, but for composite differences between QBO phase 5 and phase 1 (purple), between phase 6 and phase 2 (green), between phase 7 and phase 3 (orange), and between phase 8 and phase 4 (red) during the extended winter (November–March). The MME is shown with a filled circle and the reanalysis as a square for clarity. The plus (cross) sign denotes the composite value of the *x*- (*y*-)axis at the 95% confidence level. The font/marker color denotes the composite phases, and the number above the scattered point marks the data source. The multi-model correlation between each pair of variables (*R*) and its significance level (*α*) are also printed in each plot.

Accepted for publication in *Journal of Climate*. DOI 10.1175/JCLI-D-19-0663.1.

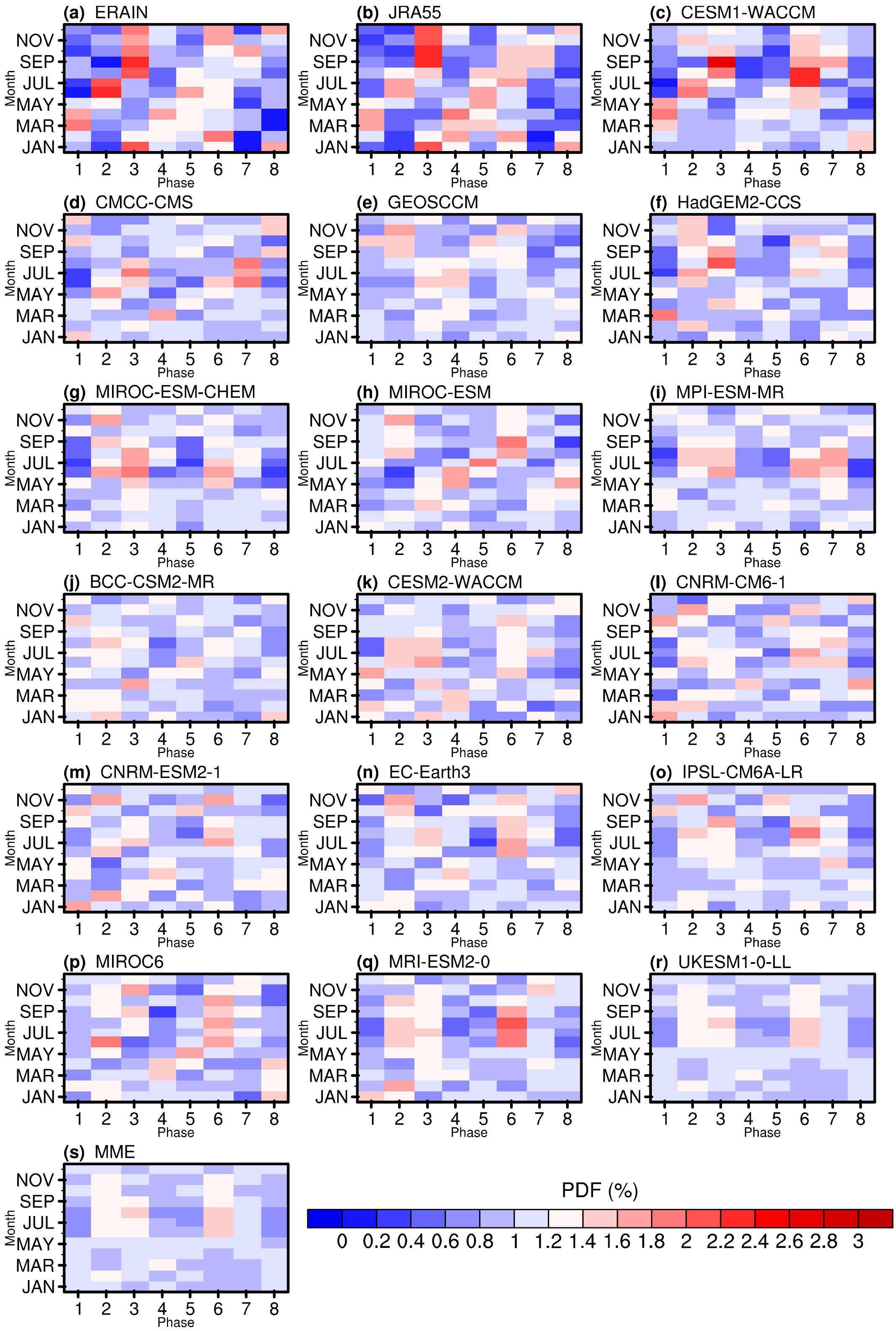

Fig. 11. The two-dimensional Probability Distribution Function (PDF) of the monthly QBO30 index as a function of the QBO phase (*x*-axis) and month (*y*-axis) for (a, b) the two reanalyses, (c–r) 16 CMIP5/6 models, and (s) multimodel ensemble (MME).

Accepted for publication in *Journal of Climate*. DOI 10.1175/JCLI-D-19-0663.1.